TECHNISCHE UNIVERSITÄT WIEN

Associate Professor Dipl.-Ing.Dr.techn. Andreas Limbeck

# Diplomarbeit

## Spatially resolved quantification of the 5-HT2A receptor in brain tissues using praseodymium labelled antibodies in combination with LA-ICP-MS detection

Ausgeführt am Institut für
Chemische Technologien und Analytik
der Technischen Universität Wien

Unter der Anleitung von
Associate Professor Dipl.-Ing. Dr.techn. Andreas Limbeck

durch
Nicole Puffler, BSc-
Mat.Nr. 01126835
Gusindegasse 26
2361 Laxenburg

Wien, April 2019

Nicole Puffler, BSc.

# Abstract

Depression is a commonly occurring mental disease. Its therapy is carried out with medication as well as with psychotherapy. The family of 5-HT receptors has an important part for that because the effect of antidepressants can be enhanced by modulation of certain serotonin receptors. For example, a range of antidepressants and antipsychotics bind to the subcategory of 5-HT2A receptors. They are mainly located in the whole central nervous system.

In the last years the interest in representing the distribution of elements is growing rapidly. It helps to define different processes more closely and helps to gain fundamental information. Therefore, it is relevant to know the distribution of these serotonin receptors.
One opportunity to gain this information is found in immunohistochemistry. It is a simple and powerful technique. To represent the distribution, an antibody reacts specifically with the analyzed receptor. For visualization the primary antibody is detected directly or indirectly. For the direct method the primary antibody is tagged, for the indirect method a secondary antibody binds to the primary. The tag is either an enzyme or a fluorophore. Notwithstanding, this part is a limiting step because it is not always possible to find a suitable opportunity of visualization. In this work the 5-HT2A receptor is used as an example. An immunohistochemical assay is used with an indirect visualization using a secondary antibody that is tagged with a fluorophore. Following, an image of the distribution is created with a fluorescence microscopy.

Since there is a limitation using immunohistochemistry, an alternative method is needed: With laser ablation inductively coupled plasma mass spectrometry (LA-ICP-MS) it is possible to extend the range of representable receptors. For the purpose of unambiguous association of the selected receptor, it has to bind specifically to a labelled antibody. It is labelled to an element that is not naturally occurring in the tissue. For this reason, the rare earth element praseodymium is selected. Now it is possible to gain information about the distribution of this special serotonin receptor by representing the distribution of praseodymium with LA-ICP-MS. Nevertheless, there are some problems for this analytical method. During the measurement

there is not only a change in the composition of the sample matrix but also variations in the experimental conditions. For this reason an internal standard is used and it has to grant a variety of requirements. It does not solve these problems it offers a possibility to take them into account. However, it has to meet some requirements. The elements gold and indium are candidates, whereas gold is applied as an additional layer on the sample and indium is present as a thin layer on the sample slides. Finally, indium turns out to be the better choice.

To quantify the results from LA-ICP-MS, all kinds of approaches exist. In many cases either certified reference material or matrix matched standards are used. Nevertheless, these two opportunities are either barely available or it is a time-consuming procedure and not easy in handling. To avoid these problems, standards are used that simulate the analyzed tissue. Since the analyzed tissue is brain, gelatin is used because it imitates animal material. For the gelatin standards, the rare earth elements lanthanum, cerium, praseodymium and europium are used. They make it possible to quantify the distribution image of the 5-HT2A receptor.

# Kurzzusammenfassung

Die Depression ist eine häufig auftretende mentale Krankheit. Die Behandlung kann sowohl medikamentös als auch mit psychotherapeutischen Ansätzen erfolgen. Die Familie der 5-HT-Rezeptoren ist dafür von wichtiger Natur, da durch Modulation bestimmter Serotoninrezeptoren die Wirkung von Antidepressiva gesteigert werden kann. So binden zum Beispiel zahlreiche Antidepressiva und Antipsychotika an den 5-HT2A-Rezeptor. Diese Unterkategorie kommt nahezu im gesamten zentralen Nervensystem vor.

Das Interesse an Darstellungen von Verteilungen von Elementen hat sich in den letzten Jahren deutlich vermehrt. Damit können nun verschiedenste Prozesse besser nachvollzogen und fundamentale Informationen erhalten werden. Aus diesem Grund ist es auch notwendig, die Verteilung dieser Serotonin Rezeptoren zu kennen.
Eine Möglichkeit bietet die Immunohistochemie, welche zugleich eine einfache und leistungsstarke Technik ist. Um nun die Verteilung darzustellen, reagiert ein Antikörper spezifisch mit dem zu analysierenden Rezeptor. Für die Visualisierung wird der primäre Antikörper entweder direkt oder indirekt detektiert. Bei der direkten Methode wird der primäre Antikörper markiert und bei der indirekten Methode bindet ein markierter sekundärer Antikörper an den primären Antikörper. Als Markierung kann entweder ein Enzym oder ein Fluorophor verwendet werden. Allerdings ist dieser Schritt ein limitierender, da nicht immer eine geeignete Möglichkeit zur Visualisierung gefunden werden kann. In dieser Arbeit wird der 5-HT2A Rezeptor als ein Beispiel verwendet. Es wird ein immunohistochemischer Analyse mit indirekter Visualisierung verwendet, für die ein sekundärer Antikörper mit einem Fluorophor markiert ist. Anschließend wird eine Darstellung zur Verteilung mit einem Fluoreszenzmikroskop erstellt

Da es zu Limitierungen kommt wenn man die Immunohistochemie verwendet, benötigt man eine Alternative. Der Bereich an darstellbaren Rezeptoren kann mittels laser ablation inductively coupled plasma mass spectrometry (LA-ICP-MS) erweitert werden. Um nun eine eindeutige Zuordnung des ausgewählten Rezeptors zu erhalten, muss dieser an einen Antikörper binden, der eine Markierung (Label) besitzt. Aus diesem Grund wird die seltene Erde Praseodym ausgewählt. Nun ist es möglich Informationen über diesen speziellen

Serotonin Rezeptor zu erhalten, in dem die Verteilung des Praseodyms mit LA-ICP.MS dargestellt wird. Jedoch treten bei dieser analytischen Methode eine Reihe von Problemen auf. Während der Messzeit können nicht nur Schwankungen in der Probenzusammensetzung auftreten, sondern es können sich auch instrumentelle Parameter ändern. Aus diesem Grund muss ein interner Standard verwendet werden, der eine Vielzahl an Voraussetzungen erfüllen muss. Dieser löst das Problem zwar nicht, bietet aber eine Möglichkeit dieses zu berücksichtigen. Auf jeden Fall muss der interne Standard einige Bedingungen erfüllen. Für diese Experimente, kommen die Elemente Gold und Indium in Frage, wobei Gold als zusätzliche Schicht auf die Probe aufgetragen werden muss und Indium als dünne Schicht am Probenträger vorhanden ist. Schlussendlich hat sich herausgestellt, dass Indium die bessere Wahl ist.

Zur Quantifizierung der Methode gibt es verschiedenste Ansätze. Sehr häufig werden entweder zertifizierte Referenzmaterialien oder Matrix angepasste Standards verwendet. Diese sind jedoch entweder kaum verfügbar oder zeitaufwändig und bieten keine leichte Handhabung. Um diese Probleme zu vermeiden, können Medien verwendet werden, die das zu untersuchende Gewebe simulieren. Da das zu analysierende Gewebe Gehirn ist, kann Gelatine verwendet werden, da damit Tiergewebe simuliert werden kann. Für diese Gelatine-Standards wurden die seltenen Erden Lanthan, Cer, Praseodym und Europium verwendet. Diese machen es auch möglich die Darstellung der Verteilung des 5-HT2A Rezeptors zu quantifizieren.

# Danksagung

An dieser Stelle möchte ich mich bei all jenen bedanken, die mich während des Studiums und dieser Arbeit unterstützt und motiviert haben. Zuerst gebührt mein Dank Andreas Limbeck, der mir nicht nur die Möglichkeit gegeben hat, Teil dieses Projekts zu sein, sondern mich immer gut betreut und beraten hat. Ich möchte mich für die hilfreichen Anregungen und konstruktiven Kritiken herzlich bedanken. Des Weiteren ein Dankeschön an Prof. Rupert Lanzenberger, von der Medizinischen Universität Wien, der dieses Projekt in die Wege geleitet hat. Zudem möchte ich mich bei Martina Marchetti-Deschmann und Victor Weiss bedanken, die mich bei diversen Fragestellungen und Equipment-Engpässen unterstützt haben.

Da man im Laufe eines Studiums nicht nur Erfolge hat, die man genießen will, sondern auch Misserfolge erlebt, die überwunden werden müssen, möchte ich mich bei meinen Studienkollegen bedanken, die mich durch diese Zeit begleitet haben. Diesen Dank möchte ich an meine Freunde weitergeben, die mich zwar oft nicht verstanden, dafür aber umso mehr unterstützt und motiviert haben.

Mein ganz besonderer Dank gilt meiner Familie, insbesondere meinen Eltern, die es mir ermöglicht haben eine schulische und akademische Laufbahn nach meinen Wünschen einzuschlagen und mich dabei auch immer mit ganzem Herzen unterstützt haben. Meiner Schwester und meinem Freund möchte ich dafür danken, dass sie immer für mich da sind.

Zum Abschluss möchte ich noch ein Zitat anführen, welches ich erst vor kurzem gelesen habe und mich seitdem anders auf Misserfolge blicken lässt:

„Erfolg ist die Fähigkeit, von einem Misserfolg zum anderen zu gehen, ohne seine Begeisterung zu verlieren."

Winston Churchill

# Table of Contents


Abstract ..... i

Kurzzusammenfassung ..... iii

Danksagung ..... v

1. Introduction ..... 1

2. Theoretical aspects ..... 5

   a. Inductively coupled plasma mass spectrometry (ICP-MS) ..... 5

      i. Sample introduction ..... 5

      ii. Inductively coupled plasma ..... 6

      iii. Interface and ion optics ..... 7

      iv. Mass Analyzer ..... 9

      v. Detector ..... 10

   b. Laser ablation (LA) and coupling with ICP-MS ..... 10

   c. Imaging experiments ..... 12

   d. Quantification ..... 14

      i. Gelatin Standards ..... 14

      ii. Internal Standard ..... 17

   e. Immunohistochemistry (IHC) ..... 18

3. Experimental ..... 21

   a. Chemicals and Reagents ..... 21

   b. Instrumental ..... 23

      i. LA-ICP-MS ..... 23

      ii. Cryotom ..... 24

      iii. Sputter coater ..... 25

   c. Gelatin Standards ..... 25

      i. LA-ICP-MS measurements ..... 27

      Statistical tests (Pearson and Hartley) ..... 28

   d. Immunohistochemistry ..... 29

      i. Sample preparation ..... 29

      ii. Fluorescence microscopy ..... 30

      iii. Chemicals ..... 31

   e. Metal tagging ..... 32

      i. Preparation ..... 32

4. Results and discussion ..... 35

   a. Indium and gold as an internal standard ..... 35

b. Quantification with REE Gelatin Standards ..... 41
c. Receptor detection ..... 45
5. Conclusion and Outlook ..... 50
Appendix ..... 54
Figures ..... 60
Tables ..... 60
Literature ..... 61

# 1. Introduction

There is a growing interest in representing the distribution of elements. It helps to improve the understanding of different processes and provides fundamental information about the sample properties. Especially, for biological or medical applications the depiction of distribution of analytes can be of special interest. As a current example, depression is a commonly occurring mental disease. Its therapy is carried out with medication as well as with psychotherapy.

The family of 5-HT receptors has an important part for that because the effect of antidepressants can be enhanced by modulation of certain serotonin receptors. A range of antidepressants and antipsychotics bind, for example, to the 5-HT2A receptor. This subcategory is located approximately in the whole central nervous system (nerval structures of the brain and the spinal cord). To generate the distribution of this receptor several methods are available.

One opportunity is found in immunohistochemistry. With this method it is possible to detect cellular components. The process is described in the following way; an added primary antibody reacts specifically with the analyzed receptor. There are two methods for visualization: it is possible to detect the primary antibody directly or indirectly. The direct method needs a primary antibody that is tagged. A limitation is the lower sensitivity. It is only possible to detect a high expressed antigen. Nevertheless, an advantage is found in the ease of use, because no additional incubation step is needed and the elimination of non-specific binding of a secondary antibody. For the indirect method a tagged secondary antibody that has a high specificity to bind with the primary antibody is used. This method has a higher level of sensitivity and generates more intensive signals because it is possible that at least two secondary antibodies bind to one primary antibody. [1] The used tag is either a fluorophore or an enzyme.

The visualization part is the limiting step because it is not always possible to find a suitable way for making the detection visible - especially, if multiple staining is performed. To detect more than one target, primary antibodies are essentially needed that are raised in different species. This prevents cross-reactivity of the secondary antibody. Since the antibody sources

are limited (rat, goat/sheep, three – four mouse isotypes and rabbit) the choice for a primary antibody is limited as well. Therefore, it is necessary to develop strategies to stain antibodies raised in the same species. There are mainly three different ways: bleaching the primary antibody before adding another layer, removing the antibodies from the section after staining and imaging or blocking the antibody before the second staining layer. Most of these methods have high costs of the tagged antibodies or can only stain a few at the same time. The opportunities for multiple staining may change because of the "next generation IHC" including in situ mass-spectrometry detection. [2] Another disadvantage is that quantification is only possible if the amount of used antibody is in a controlled range and non-specific staining is avoided. If these requirements are made, the fluorescence signal response will be linear and useful to quantify the selected region. [3]

For this reason, an alternative method is wanted. With laser ablation inductively coupled plasma mass spectrometry (LA-ICP-MS) it is possible to extend the range of representable receptors. Nevertheless, there are some problems for this analytical method. During the measurement there is not only a variation in the experimental conditions but also a change in the composition of the sample matrix. This may lead to changes in absolute signal intensities. Consequently, an internal standard is needed, that considers all these factors. Certainly, it has to grant a variety of requirements. The internal standard and the analyzed element should have comparable behavior during transportation, ablation and concentration. There are two different types: it is naturally occurring in the sample. For biological samples carbon is the most prominent example. Unfortunately, a problem is found in the high first ionization energy because drastic signal changes may occur if the plasma conditions only changes negligible. For this reason, it is only suitable under certain conditions. The other type is applied on the sample surface.

For this experiment there are two possible solutions. One possibility is gold. It is often used and was tested by Konz.et al. [4] with satisfying results. It has to be applied as a homogenous film through a sputtering process. Another candidate is found in indium that is present as a thin layer on the sample slides. Since there is no additional step for applying indium on the sample, it would facilitate the workflow. Another benefit that it is not possible to carry in

contaminations that lead to interferences. This indium tin oxide has a thickness of 150 – 300Å.

To quantify the method, standards have to be prepared. In general, all kinds of approaches exist to quantify a method. In many cases matrix matched standards or certified reference material are used.

- Certified reference material: there is a detailed certificate with the components and their concentrations. It offers high accuracy and precision. Unfortunately, for biological samples it is only possible to get powder materials which are not suitable for these experiments. Nevertheless, this procedure is time consuming and not easy in handling.
- Matrix-matched standards: one major proponent is that the preparation is individually and that the concentration rage is selected customized. For. brain matrices there is a procedure tested from Hare et al. [5] but it is time consuming and not easy in handling.

As an alternative standards are used that simulated the analyzed tissue. In this work the analyzed tissues are brains of rats. Gelatin gels are selected to prepare the standards because they imitate animal material.

As standards some of the rare earth elements (REE) were used: lanthanum, cerium, praseodymium and europium. One proponent is that they have no or less isobaric interferences. After the gelatin gels are prepared they are analyzed using LA-ICP-MS. Therefore the spot scan mode is used: the laser fires onto one spot of the sample for a defined time, stops and the ablated material is washed out of the ablation chamber and transported into the ICP-MS. If this process is ended it moves to the next position to ablate. A special pattern has to be designed to detect different places on the sample. Since there are still physical and chemical differences between sample and standard an internal standard is needed. After the measurement the data has to be normalized by dividing the analyte signal by the corresponding internal standard signal.

To generate the distribution with LA-ICP-MS of the receptor it has first to react specifically with an antibody. For the purpose of unambiguous association of the receptor in the image, it is essential to tag an element to the antibody that is not naturally occurring in the used tissue (brain of rats). For that reason, the rare earth element praseodymium was chosen. It has no isobaric interferences and to enhance the sensitivity because of their low ionization potential.[6]

The labeling process is accomplished by using a labeling kit from Fluidigm. The labeling procedure involves first loading the polymer with the rare earth praseodymium, then partially reducing the antibody and finally conjugating the antibody with the lanthanide-loaded polymer. Afterwards the labelled antibodies should be applied on the cut sample that is placed on an ITO-slide.

The sample is then analyzed using LA-ICP-MS. Therefore, another mode should be used: the line scan. The laser fires on the sample and moves with a given scan speed in one direction. After the washout time the laser moves to the second line. A negative aspect is that the resolution suffers because of blurring effects of neighboring spots but in comparison to the aforementioned spot scan, it is more time efficient. This reason makes the line scan attractive for image creations. Nevertheless, there is one important aspect that has to be kept in view: during the ablation process it is possible that there is a time-dependent change in the elemental ratios. That originates from the fact that the plasma needs to reach the equilibrium until a continuous flow of ablated material is accomplished. This effect is primary observable at the beginning of a line scan and has to be taken into account.

In this work the imaging process with LA-ICP-MS should not only show the distribution of the analyzed receptor but as well give quantitative information. For this reason, the standard series of praseodymium should be consulted.

## 2. Theoretical aspects

### *a. Inductively coupled plasma mass spectrometry (ICP-MS)*

Inductively Coupled Plasma Mass Spectrometry (ICP-MS) is a widely used analytical method for elemental analysis. It is used in many fields such as environmental and life science, geology, also in semiconductor and food industry. For example geochemical analysis labs are using this method because of its detection capabilities, especially for the rare-earth elements (REE). [7]

The strength lies in a wide elemental coverage, a high sensitivity and a high dynamic range. Major advantages are a linear range (8-11 orders of magnitude [8]), low detections limits (from low pg/mL to high µg/mL for almost all elements [9]) and a multi elemental detection including isotopic information. These advantages make this method to a favorite for inorganic trace- and ultra-analysis.

Figure 1 shows a schematic view of an ICP.

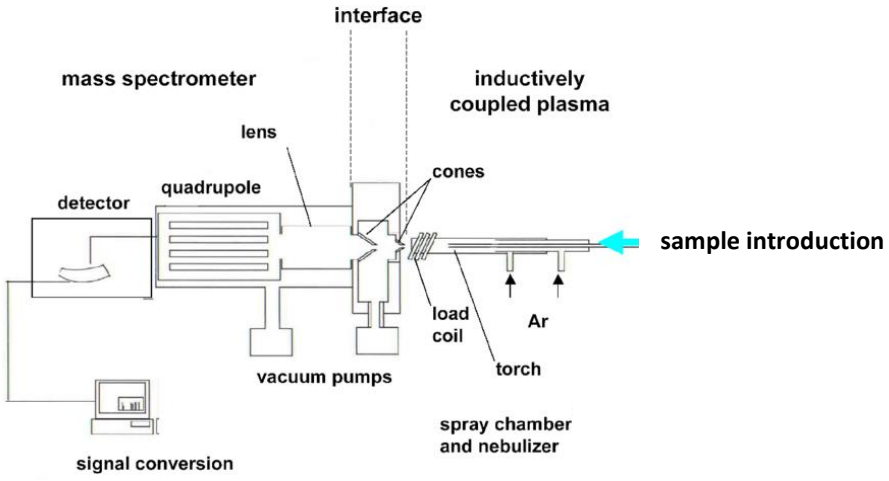


*Figure 1: Schematics of an inductively coupled plasma mass spectrometer (ICP-MS)* [10]

#### *i. Sample introduction*

In most cases the sample is introduced as a liquid. Therefore a nebulizer is needed (see Figure 2). Its function is to transfer the sample into an aerosol and to transport it into the plasma. For the direct introduction of solid samples there are various techniques, for example the laser ablation, which will be described later.

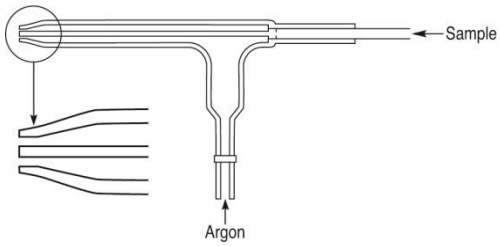


*Figure 2: Schematic of a nebulizer* [11]

### *ii. Inductively coupled plasma*

The inductively coupled plasma (ICP) is one of the most used sources for ionizations for inorganic mass spectrometry.

After a solid or liquid sample is transformed into an aerosol it is transported directly into the plasma. With a carrier gas the aerosol is transported through the inner tube of the plasma torch and then introduced into the argon plasma. Depending on the temperature several processes take place.

The ICP-torch consists of three quartz tubes (see Figure 3: ICP left: concentric quartz tubes [3]), which are disposed concentric and are flushed with Argon at different flow rates and an induction coil on the top. The power of the coil is between 750 and 1700 W [3]. The used frequency is either 27.1 MHz or 40.6 MHz [13]. The oscillations lead to electrical and magnetic fields at the top of the torch. With a spark electrons are stripped from some Argon-atoms. They get trapped in the magnetic field and are accelerated. Then these fast electrons collide with neutral Argon atoms and $Ar^+$ ions are formed. This process is called "inductively coupling".

This process of collision leads to the high temperatures of the plasma. Depending on the region, the temperature of the plasma is between 6000 and 10 000 K and, therefore, the aerosol is first desolvated then vaporized, atomized (break of chemical bonds) and finally ionized if the first ionization energy is smaller than 15.76 eV (first ionization energy of Argon [9]). The plasma exists as long as the induction coil provides energy.

As mentioned before, the torch consists of three concentric tubes with different argon flows. The outermost one is streamed with coolant gas with a flow rate of 11 to 15 L $min^{-1}$. It has a tangential flow to keep the plasma away from the walls of the quartz torch. This is

the reason why the plasma has a droplet shape. The middle one is the auxiliary flow with a flow rate of 0.5 to 1.5 L $min^{-1}$. Its aim is to prevent the plasma from melting the innermost tube. The sample passes through the innermost channel with an Argon flow rate of 0.5 to 1.5 L $min^{-1}$ and is often called “nebulizer gas flow”. [9]

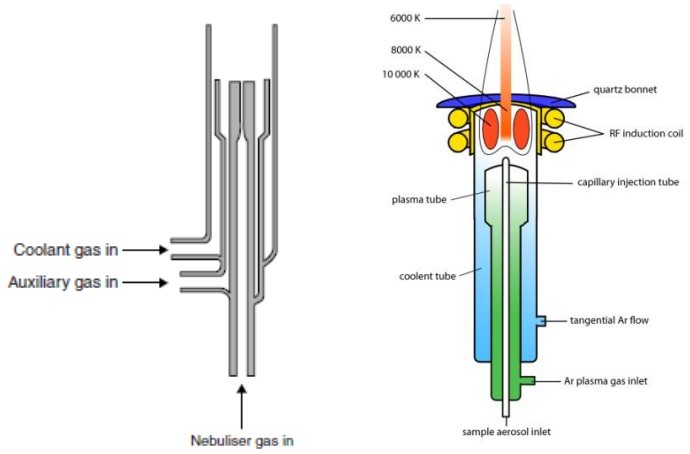


*Figure 3: ICP left: concentric quartz tubes [3] right: schematic diagram* [12]

### iii. *Interface and ion optics*

The detection of separated ions takes place at reduced pressure ($10^{-5}$ – $10^{-9}$ mbar) in the mass spectrometer. This condition leads to a reduced amount of gas molecules and therefore fewer collisions with analyte ions. Since the ICP provides an atmospheric pressure an interface which extracts the analyte ions is needed. A very high change of the pressure is handled in a very short range. This interface is a very difficult part of the ICP-MS.

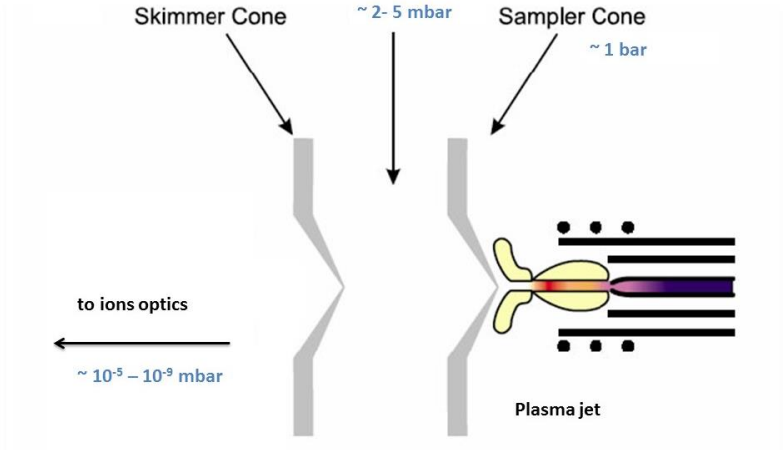


*Figure 4: ICP MS vacuum interface* [13]

As seen in Figure 4, the interface consists of two parts: in the front there is the sample cone and behind the skimmer cone. Both usually consist of nickel but sometimes other metals like aluminum, copper or platinum are used for special applications. After the sample cone there is an expansion chamber where a rotary pump produces a pressure of 2 – 5 mbar. Afterwards the step into the high vacuum is accomplished from the skimmer cone which has a smaller aperture diameter (0.7-0.4 mm) than the sample cone (1.0-0.5 mm) with a turbomolecular pump.
It should be mentioned that this transport into the high-vacuum causes a high loss of the ions. The reason can be found in the expansion of the ion beam from normal to reduced pressure. In compensation an ion optics is used.

The ion optics consists of one or more electrostatically controlled lenses. They are positioned between the skimmer cone and the mass analyzer section. One important function is to focus the ions after transition from atmospheric pressure to high vacuum to avoid fractionation effects. Another important role of the ion optics is to stop neutral species and photons from entering the mass analyzer because they cause signal instability and a high background level.

iv. *Mass Analyzer*

The ions are separated and detected by the mass spectrometer (MS). There are three different types that are available: the sector field mass spectrometer, the time-of-flight (TOF) mass spectrometer and the quadrupole mass spectrometer. Since the quadruple MS was used in this work it will be described in detail.

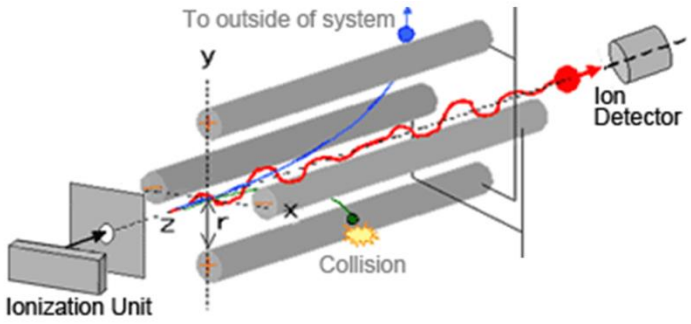


*Figure 5: Overview of a Quadrupole MS [14]*

The quadrupole MS consists of four metallic and parallel rods with a hyperbolic cross section, where two opposite rods have the same polarity. The electrical fields generated by the rods have an effect to the trajectories of the travelling ions. For a given voltage only ions of a certain mass-to-charge ration (m/z) pass through the quadrupole filter because if the potential of the ion is higher than of one pair of rods, it will be attracted, otherwise it will be repulsed. At certain settings, ions of a particular m/z-ration will oscillate with a trajectory that is between the rods and reach the detector (see schematic drawing in Figure 5). By changing the voltages, the analyzed m/z ratios can be varied in a very short time.

It should be mentioned that there is a problem with interferences because it could be possible that there is a species with an m/z ratio that cannot be separated from the analyte ion.

Interferences can appear because of:

- isobaric species, for example $^{40}Ar$ and $^{40}Ca$
- multiple charged ions, for example $^{64}Zn^{2+}$ and $^{32}S$ or
- polyatomic ions especially oxides and argides ($^{151}Eu$ = $^{135}Ba^{16}O^{+}$, $^{153}Eu$ = $^{137}Ba^{16}O^{+}$ )

In some cases, these interferences cannot be separated from the analyte. Especially the quadrupole MS offers only a lower mass resolution. This problem can be compensated using a collision chamber.

#### *v. Detector*

Detectors are used to convert the ion current into countable pulses. The two most used are the electron multiplier and the Faraday cup.

An electron multiplier works with the physical effect of secondary electron emission. The analyte ion impinges on a surface where it obtains a secondary electron from a surface atom. They are accelerated and hit again a surface and more electrons are released so that the signal is intensified. For mass spectrometry there are two basic forms: the discrete-dynode and the continuous-dynode electron multiplier.

When the metal cup in the Faraday cup catches a beam of charged particles (ions or electrons), it gains a net charge while the ions or electrons are neutralized. The current that flows through the circuit can be measured and is directly proportional to the number of incoming ions. Around the cup there is a cage that protects the secondary electrons to leave the detector.

## *b. Laser ablation (LA) and coupling with ICP-MS*

The combination of laser ablation (LA) with inductively coupled plasma mass spectrometry (ICP-MS) is a potent technique for the elemental analysis of solid samples. One major advantage of this method is that sample preparation steps like dissolution are not needed so that slightly soluble materials like carbide, oxides are easily analyzed and that distribution analysis can be realized.

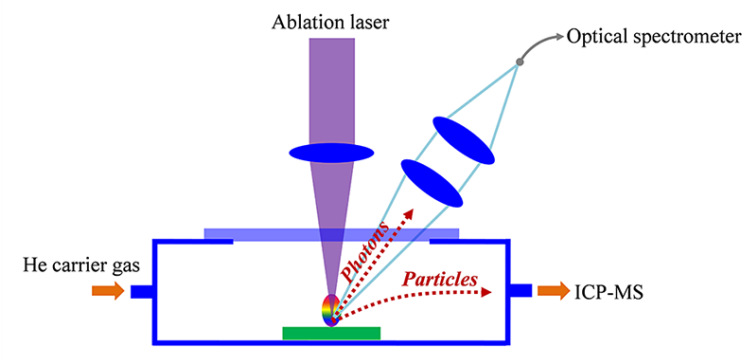


*Figure 6: Schematic of a laser ablation unit* [15]

Figure 6 shows a schematic of a laser ablation unit that is ether coupled to an ICP-MS or an ICP-AES (Atomic-Emission-Spectroscopy). It basically consists of an ablation chamber which is flushed by an inert gas (in most cases Helium) with a sample stage that allows the translation in x, y and z direction, the carrier gas (noble gas like Helium) which flushes the sample chamber and the laser. To correctly select the region of interest, a microscope is integrated into the ablation chamber.

The laser (**L**ight **A**mplification by **S**timulated **E**mission of **R**adiation) is focused on the sample and emits monochromatic light that interacts with the surface so that an aerosol of small particles, ions and atoms are removed from the outermost layers, is formed. Further it is transported with an inert gas stream (in most cases Helium) to the ICP-MS. With this laser ablation system both analysis with low spatial resolution (> 100 µm) for bulk analysis and local analysis with a high spatial resolution (< 20 µm) are realizable. [9] Overall it reaches a high sensitivity so that this analytical system is used for trace analysis.

There are different laser types that are most commonly classified by the material. One group is defined as solid state lasers. A prominent example is the Nd:YAG laser (Neodymium doped yttrium aluminium garnet, Nd-$Y_3Al_5O_{15}$) which works in the IR region (most powerful at 1064 nm [9]) or in the UV region (for example 532 nm [9]). Another group is formed with gas lasers where light is produced in the UV range.

The used wavelength has an important influence on the process: with lower wavelengths the energy density on the sample increases. In general, lower laser wavelengths in the ultra violet (UV) region are used because of their interaction with the sample. For example:

a laser working in the UV-region leads to a good ablation for a glass material whereas a laser in the IR regions mostly melts it.

Pulsed lasers are typically used with a pulse length between nano- to the femtosecond range. The ablation mechanism for pulses in nanosecond range is dominated by thermal effects so that the laser crater is not as sharp as with shorter pulse duration. The occurring melting effects lead to unconstant ablation efficiency for the elements of the sample.

The lateral resolution is accompanied with the spot size. To control the spot size of Nd:YAG lasers the laser focus and the incident energy have to be matched.

### *c. Imaging experiments*

Over the last years there is a growing interest in imaging mass spectrometric techniques for biological and medical uses. There the distribution of metals, metalloids and non-metals in biological samples is of major focus. This process of visualization is called imaging. Especially the research of metalloproteins in brain tissues have gained a lot of knowledge since neurodegenerative diseases like the Alzheimer's or tumor growth are used for imaging experiments. It is a powerful method because it produces quantitative images with a detailed regionally specific element distribution. It helps to improve the understanding of different processes and provides fundamental information about the properties. Another benefit is that quantification is possible if there is a suitable calibration standard.

For this work imaging was accomplished with laser ablation and inductively coupled plasma mass spectrometry. It should on one hand show the elemental distribution on the sample surface and on the other hand it should also give quantitative information about the analytes.

There are two modes of ablation available: the line scan and the spot scan (see schematics in Figure 7).

If the spot scan is used, the laser fires onto one spot of the sample for a defined time. After the laser stops, the ablated material is washed out of the ablation chamber and transported into the ICP-MS. If this process is ended it moves to the next position to ablate. After every spot a pause is needed what makes this mode to a time-consuming technique. The other method is the line scan where the laser fires on the sample and moves with a given scan speed in one direction. After the washout time the laser moves to the second line. Furthermore, the resolution suffers because of blurring effects of neighboring spots. In comparison, the line scan mode is preferred because the creation of chemical images is at least as good as with spot scans but more time-efficient.

There is one aspect that has to be kept in view: there is a time-dependent change in the elemental ratios during the ablation process. The plasma needs to reach the equilibrium until a continuous flow of ablated material is accomplished but therefore some time is needed. This effect is primary observable in the starting signal of each spot or at the beginning of a line scan and has to be taken into account.

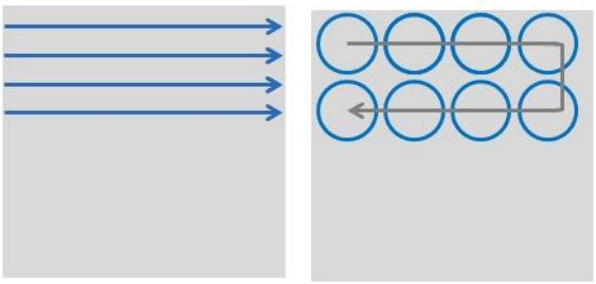

*Figure 7: Schematics of a line scan pattern (left) and a spot scan pattern (right)*

If a method is developed the parameters of the laser like scan speed, laser beam diameter, laser energy and repetition rate have to be taken into account. Whereas the repetition rate is typically up to 20 Hz, the beam size and scan speed turn out to be well-conceived parameters. As a result, the spatial resolution of the image is determined by the laser beam diameter. With a decreasing beam diameter less material is ablated and therefore less analyte is detected. This aspect can be important if it is a trace or an ultra-trace analysis since a signal above the detection limit is needed. Another considerable issue is the measurement time. If an image of a whole sample is wanted the scan speed and the

laser spot size define the measurement time. Depending on the biological sample and the wanted spatial resolution typical diameters are between 10 and 100 µm.

Figure 8 shows a typical diagram that is generated by the software during the imaging process. At first the signal intensity is plotted against the time. Considering the imaging parameters, the time axis can be converted into a length axis.

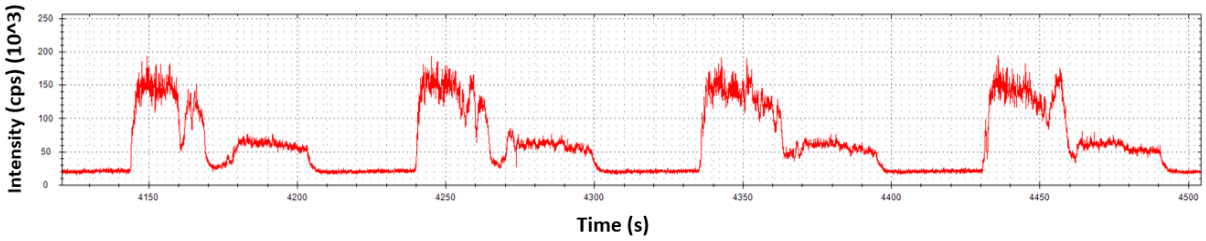


*Figure 8: Software generated diagramm*

## *d. Quantification*

The ablation is not similar for all kind of samples. To get a trustworthy quantitative determination of the composition of the sample standards have to be used.

### *i. Gelatin Standards*

For imaging with LA-ICP-MS there are some problems in quantifications since there is a lack of reference material. The most reliable method is the use of certified reference materials (CRM). They are extensively characterized and a detailed certificate with the concentrations of the components is readily available. If they are used correctly they provide high precision and accuracy. Nevertheless, for many samples like biological or medical ones there are no CRMs for imaging experiments. There are only available as powder for bulk material. Consequently, alternatives are used.

Another way of quantification is the preparation of standards which are prepared from the same material as the analyzed sample. They are called matrix-matched standards and they help to get a consistent ablation behavior. The preparation is individually in house with for

example different concentrations for each experiment. Consequently, standards have to be prepared for each tissue individually. For brain matrices there is a procedure tested from Hare et al. [16] but it is time consuming and not easy in handling. At first the brain has to be washed and prepared (remove residual blood fluids), then homogenized and spiked with the standards. Afterwards they were weighted, cryofixed, cut and finally mounted on glass slides. To avoid this, a tissue simulating media can be used. For example, gelatin gels are chosen to imitate animal materials. They are very popular because of their ease in use as well as preparation. [17] Another benefit is the flexible choice concerning element and concentration. Since there are still physical and chemical differences between sample and standard an internal standard is needed. [18]

Rare Earth Elements

The rare earth elements (REE) were chosen for the tagging process. Since ICP is an element analysis method, a specific tag is needed to detect the antibody that binds specific to the receptor. These elements do not naturally occur in biological samples and are good detectable. With these non-present heteroatoms as labels, it is on one hand possible to detect proteins or peptides that otherwise could not be and on the other hand enhance the sensitivity. Especially, most rare earth elements are capable to this enhancement because of their low ionization potential. [6]

The labeling procedure is shown in Figure 9 and involves first loading the polymer with lanthanide (A), partially reducing the antibody (B) and finally conjugating the antibody with the lanthanide-loaded polymer (C).

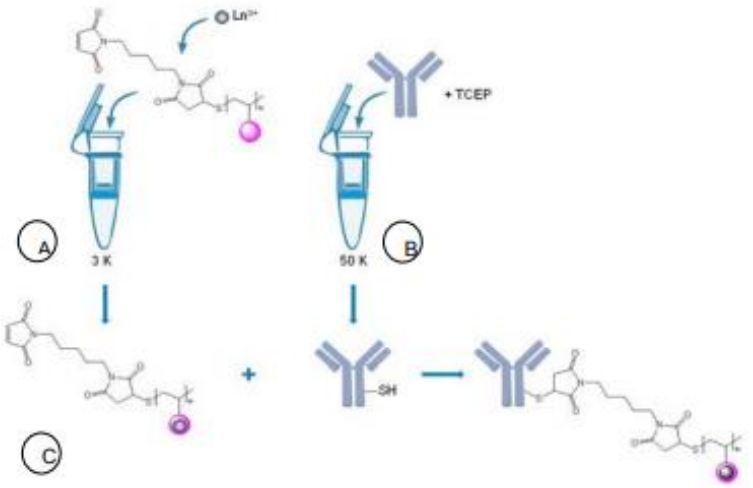


*Figure 9: Overview of the metal tagging process* [19]

The following table (Table 1) shows some characteristics of the used REE. Lanthanum, cerium, praseodymium and europium were used because they have no or less isobaric interferences (there is for just the $^{142}$Nd with a natural abundance of 27% [20]). Praseodymium has been chosen as tag because there are no singly charged isotopes that overlap with that monoisotopic element [21]. All isotopes are natural occurring and stable with the exception of $^{151}$Eu which is unstable to alpha decay with a half-life of 5*1018 years.

*Table 1 Characteristics of the used Rare Earth Elements (REE)*

| | La | Ce | | Pr | Eu | |
|---|---|---|---|---|---|---|
| Atomic number | 57 | 58 | | 59 | 63 | |
| Ionization potential (eV) [22] | 5.212 | 5.577 | | 5.539 | 5.644 | |
| Atomic weight (amu) [23] | 138.91 | 140.12 | | 140.91 | 151.96 | |
| Isotope | 139 | 140 | 142 | 141 | 151 | 153 |
| Abundance (%) | 99.91 | 88.45 | 11.11 | 100 | 47.80 | 52.20 |

### *ii. Internal Standard*

During the measurement there is a variation in the experimental conditions. Since the matrix may vary in composition and height, the laser ablation is different and the plasma condition may change. For example, the temperature changes, the conditions of the cones vary. As a result, their fields change what leads to drifts during the measurement. It is also possible that the vacuum conditions could change marginal or the gas flows change slightly. Due to instrumental drifts variations in absolute signal intensities may occur. To consider all these factors an internal standard is used because calibration strategies do not eliminate these effects. As another benefit it should be able to compensate differences between day-to-day variations to make different experiments more comparable. [18]

There are two types of internal standards. It can naturally occur in the sample or it can be applied on the surface. One prominent example of a naturally occurring internal standard is carbon which is present in every sample that has a biological origin. Since there are controversial results on whether it is a good or a bad internal standard Frick et al. [24] did some fundamental studies on the ablation behavior. They investigated that there is a formation of two phases during the experiment. One is carbon-containing gaseous and the other one a carbon-containing particle phase. Since the formation is strongly matrix depended the use of carbon as an internal standard is only appropriate under certain conditions and even there it might not be suitable. Another problem is the high first ionization potential of 11.3 eV because if the plasma condition only changes negligible, drastic changes in signal intensities may occur. Except a suitable ionization potential there are some other requirements: The internal standard element must be homogeneously distributed within the sample. It can naturally occur or added before the experiment. Furthermore, the analyzed and internal element should have similar behavior during ablation, transport and the concentrations should be comparable. For example it is important to know whether the element is transported gaseous or particulate into the ICP. [5]

Other concepts are coating the sample surface with an organic film spiked with metals like Ruthenium (Ru) and Yttrium (Y) [5] which results in a protracted time consuming sample preparation and the use of a gold layer. This method has been tested by Konz et al [4] with

satisfying results. They deposited a homogenous thin film of gold on the tissue surface as internal standard and used the $^{197}Au^{+}$ signal for normalization. With this procedure they got better quantification results. Moreover, the sample preparation is not time consuming what makes this new method an improvement.

As mentioned before the sample preparation is not very difficult. A thin layer can be homogenously applied on the surface with sputtering techniques in a few minutes. Moreover, the first ionization potential of gold with 9.23 eV is nearly comparable with those of the rare earth elements (e.g. Praseodymium with 5.47 eV) and it is not influenceable by spectral interferences. Normally one negative aspect is the high mass with 196.97 g $mol^{-1}$. Since the mass of the used rare earth elements ranges between 138.91 – 151.96 g $mol^{-1}$ it turns into a proponent because Finley-Jones et al. discovered that it is an important aspect to reduce the mass difference between analyte and internal standard.[25]

### *e. Immunohistochemistry (IHC)*

Immunohistochemistry (IHC) is a method for detecting cellular components for example proteins, antigens or other macromolecules in tissues. To make the analyte component visible a labelled antibody is needed that reacts specifically with the target antigen. Since there are many ways to achieve the visualization and many different protocols exist for different assays, the used method needs to be carefully optimized in view of the tissue, the target protein and antibody.

The IHC technique is routinely used in many fields in health care and in research. For example, with specific tumor markers it is possible to determine if a tumor is benign or malignant or get information of its stage. Another application is to represent the distribution of the analyte. The antibody-antigen binding can be visualized in many different ways. One opportunity is a direct method, were the primary antibody is directly conjugated to a label. The benefit is that there is no second incubation step but the antibody needs to be high concentrated. Another method is the indirect detection, where

the primary antibody is bound by a labelled secondary antibody that has a high specificity to bind with the primary antibody. The advantage is that there is a signal amplification because two or more labelled secondary antibodies can bind to each primary antibody. It is possible to label the antibody with enzymes like horseradish peroxidase or alkaline phosphatase or with a fluorophore.

The classical principle of an IHC-assay is illustrated in Figure 10. An antigen of the tissue sample binds specifically with an added primary antibody. Afterwards a secondary antibody is added that has a high specificity to bind with the primary antibody. After this antibody-antibody binding, a chemical substrate is added which leads to a colored precipitate at the antigen-antibodies-complex. The next step is to add 3,3'Diaminobenzidine (DAB) which is transformed by the HRP enzyme into a brown precipitate. With an appropriate microscope the stained cells and the distribution is visible.

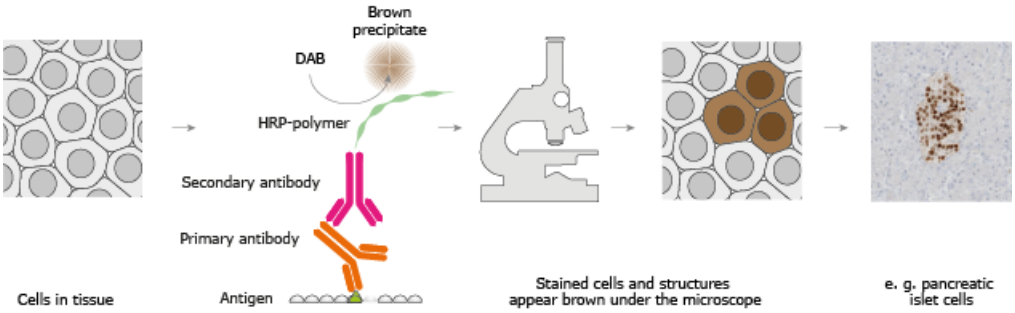


*Figure 10: Basic principle of an IHC-assay* [26]

In this work another IHC assay was used. Its process is described detailed in Chapter 3.d.i.

Even though it is a simple, good established technique, there are still some limitations, difficulties and problems. At first, the executer requires rigor of execution and interpret the results with caution. Additionally, the acquisition, handling, fixation, specimen delivery and antigen retrieval are all critical factor. As an example, it is shown that there is a loss of antigenicity depending of the specimen and the fixation. Jacobs et al. discovered that there is a significant loss at histological slices on slides stored at room temperature and 4°C after several weeks of storage. [27]. Otherwise, this is not noticeable for slides with histological specimen embedded in paraffin blocks for storage of several years. [28]

The standard is to perform one stain at a time but recently there is an interest in performing multiple assays. A problem of these experiments is the cross-reactivity between the detection reagents. To limit this problem of the secondary reagents, the primary antibodies should be raised in different species. Since the antibody sources are limited (rat, goat/sheep, three – four mouse isotypes and rabbit) the choice for a primary antibody is limited as well. Therefore, species-specific secondary antibodies are used. They recognize only the right primary antibody. [1] For this reason, it is necessary to develop strategies to stain antibodies raised in the same species. There are mainly three different ways: bleaching the primary antibody before adding another layer, removing the antibodies from the section after staining and imaging or blocking the antibody before the second staining layer. Most of these methods have high costs of the tagged antibodies or can only stain a few at the same time. The opportunities for multiple staining may change because of the "next generation IHC" including in situ mass-spectrometry detection. [2] Another disadvantage is that quantification is only possible if the amount of used antibody is in a controlled range and non-specific staining is avoided. If these requirements are made, the fluorescence signal response will be linear and useful to quantify the selected region. [3]

# 3. Experimental

## *a. Chemicals and Reagents*

ITO-Slides

For the analysis indium tin oxide coated glass slides from Sigma-Aldrich were used. They have a surface resistivity of 70 – 100 Ω/sq and a linear formula of $In_2O_3 \cdot (SnO_2)_x$. The thickness of the ITO coating is 150 – 300 $\dot{A}$.

Gelatin Standards

Table 2 gives an overview of the chemicals that were used for the preparation of the gelatin standards.

*Table 2: Chemicals used for the preparation of the gelatin standards*

| Name | Supplier |
|---|---|
| Gelatine sülle super | Neuber Chemische Fabrik W. Neuber Gesellschaft m.b.H. |
| Praseodymium emission standard (ICP-MS) | VWR Chemicals |
| Lanthanum ICP standard | Merck KGaA |
| Europium plasma standard solution | Thermo Fischer (Kandel) GmbH |
| Cerium plasma standard solution | |
| Nitric acid 65% | Merck KGaA |

Labeling

For the labeling process a labeling kit from Fluidigm and supplementary material was used. A detailed listing is given in Table 3.

*Table 3: Chemicals of the labeling kit from Fluidigm*

| Name | Supplier |
|---|---|
| R-Buffer | Fluidigm |
| C-Buffer | |
| L-Buffer | |
| W-Buffer | |
| Maxpar Polymer | |
| Praseodymium Solution | |
| Centrifugal Filter Unit: 3kDa / 50kDa Amicon Ultra 500 µL V bottom | Sigma Aldrich |
| Anti-HTR2A Antibody | |
| BioStab Antibody Stabilizer | |
| Tris(2-carboxyethyl)phosphine hydrochloride | |

For the antibody it was mandatory that it is glycerol free, carrier free (no BSA, hydrolyzed protein, no gelatin) and a purified IgG or polyclonal.

## b. *Instrumental*

### i. *LA-ICP-MS*

In this work a quadrupole ICP-MS instrumentation (Thermo Scientific iCAP Q ICP-MS, Thermo Fisher Scientific, USA,) which was coupled to a Laser Ablation device (New Wave 213 Laser Ablation device, Figure 11) was used.

*Figure 11: Thermo Scientific iCAP Q ICP-MS used for the experiments* [29]

The parameters of the measurements are listed in Table 4. Data acquisition was carried out with the software Qtegra (Version 2.10.3324.62).

*Table 4: Parameters of the ICP-MS measurements*

| | |
|---|---|
| RF-Power (W) | 1400 |
| Auxiliary gas flow (L/min) | 0.4 |
| Nebulizer gas flow (L/min) | 0.8 |
| Cool gas flow (L/min) | 12 |
| Dwell time (s) | 0.02 |
| REE | $^{139}$La, $^{140}$Ce, $^{142}$Ce, $^{141}$Pr, $^{151}$Eu, $^{153}$Eu |

The laser that was used in this work is a Nd:YAG laser. It is a Neodymium doped yttrium aluminium garnet (Nd-$Y_3Al_5O_{15}$) and it can be categorized to solid-stat lasers. To get an efficient and good working ablation process the laser properties have to be deliberately selected.

For the laser ablation the laser system ESI NWR 213 (Electro Scientific Industries, Inc Portland, USA, Figure 12) with a Nd:YAG laser was used. The frequency is quintupled to a wavelength of 213 nm. The ablation process took place under Helium atmosphere with a gas flow of 650 mL $min^{-1}$ but before entering the plasma, Argon nebulizer gas was added thereto. The ICP-MS was connected to the laser ablation device via a Teflon tube.

*Figure 12: ESI NWR 213 used for the experiments* [30]

The MS instrumentation settings were optimized by using the NIST 162 glass standard. There the signals of $^{115}In$, $^{7}Li$ and $^{238}Ur$ had to be at a maximum. The used parameters are shown in Table 5.

*Table 5: Parameters for the laser ablation for the NIST-measurements*

| | |
|---|---|
| Spot size (µm) | 80 |
| Scan Speed (µm/s) | 5 |
| Laser Energy (%) | 70 |
| Repetition Rate (Hz) | 10 |

### *ii. Cryotom*

To produce the waferthin sample slides with a thickness of 10 µm the Thermo Scientific CryoStar NX50 (see Figure 13) was used with a working temperature of -20°C.

*Figure 13: Thermo Scientific CryoStar NX50* [31]

#### *iii. Sputter coater*

To coat the samples with gold the Agar B7340 sputter coater with a gold sputtering target was used. A detailed description can be found in *"Application of gold thin-films for internal standardization in LA-ICP-MS imaging experiments"* from Maximilian Bonta. [18]

### *c. Gelatin Standards*

For the preparation of the multi element standards 3 g gelatin was mixed with 15 mL deionized water. Since the gelatin was not completely soluble the mixture was warmed up under hot water until it became clear. Afterwards 2 mL of the standard-mix was added. For that, the liquid single element standards of the rare earth elements (Cerium, Europium, Lanthanum and Praseodymium) were mixed to a 1% $HNO_3$ stock solution. Dilutions were prepared freshly out of this stock solution. In the end the gelatin standards had concentrations with 0 - 18 µg/g of each rare earth element (see Table 6 and Table 7). After the mixture was clear and free of bubbles it was cured overnight in a culture dish.

At first the sample material has to be cut into thin section because the uncut sample is not suitable for the ablation chamber. Therefore, a cryotome was used which works under frozen temperatures about -20°C. Typical thicknesses of the cut tissues are between 10 and 100 µm. Afterwards the sections were placed on ITO-slides. To get the best quantitative information the tissue should be completely ablated which was achieved in

this work with sections that are 10 µm thick. To verify if the material is completely ablated a second laser shot was fired on the previous shot. If the spectrum shows no cerium, europium, lanthanum, praseodymium and indium it can be gathered that the material is ablated completely. In some cases, they were sputtered with a thin gold layer.

*Table 6: Concentration of the REE gelatin standards for the comparison of the internal standards*

| La (µg/g) | Ce (µg/g) | Pr (µg/g) | Eu (µg/g) |
|---|---|---|---|
| 0.5007 | | | |
| 1.0027 | | | |
| 2.0007 | | | |
| 3.9987 | | | |

*Table 7: Concentration of the REE Gelatin Standards for quantification*

| La (µg/g) | Ce (µg/g) | Pr (µg/g) | Eu (µg/g) |
|---|---|---|---|
| 0.299 | 0.300 | 0.299 | 0.302 |
| 0.613 | 0.615 | 0.612 | 0.620 |
| 1.240 | 1.244 | 1.238 | 1.253 |
| 2.482 | 2.491 | 2.479 | 2.510 |
| 4.929 | 4.946 | 4.924 | 4.984 |
| 9.365 | 9.399 | 9.356 | 9.470 |
| 18.663 | 18.730 | 18.645 | 18.873 |

Since the standards of Table 6 were only used for the comparison of Indium and Gold as internal standard, it was sufficient to calculate the concentration through the weighed gelatin. On the contrary the concentrations of Table 7 were determined more exactly. A defined amount of the gelatin standards was dissolved in a $H_2O_2/HNO_3$ solution in a water bath at 60°C for one hour. Afterwards Indium was added as internal standard and the concentration was determined with an ICP-MS measurement.

### *i. LA-ICP-MS measurements*

The preparation of the sample is crucial. Tissues must be in thin slices. There are various methods for the preparation step. The most common is formalin fixation and paraffin embedding. Afterwards they are cut with a cryotome. In this work the original tissue was cut while it was frozen with the cryotome into slides with a thickness of 10 µm and were then put onto the ITO-slides. Since they were cut at -20°C they had to thaw to room temperature. If it was needed (for the experiments concerning the internal standard) the next step was applying the gold layer.

For the LA-ICP-MS experiments the parameters had to be optimized (see Table 8). For the imaging experiments a compromise between laser diameter and time had to be found. The used parameters are shown in Table 8.

*Table 8: Parameters for the LA-ICP-MS experiments*

| | Spot scan | Line scan |
|---|---|---|
| Spot size (µm) | 20 | 50 |
| Laser energy (%) | 60 | 60 |
| Repetition rate (Hz) | 10 | 20 |
| Scan speed (µm/s) | - | 150 |

To warm the laser adequately up, it was switched on before the experiment. Then samples were placed on a sample stage, flushed for 10 minutes with helium before the plasma of the ICP-MS was initialized. After half an hour warm up time the experiment was started.

The isotopes $^{115}$In, $^{139}$La, $^{140}$Ce, $^{141}$Pr, $^{142}$Ce, $^{151}$Eu, $^{153}$Eu and $^{197}$Au were monitored and the samples were scanned using a five-spot-pattern (see schematic drawing in Figure 14) which was equally distributed on the sample ten times or a line scan which covered the whole sample. The analyte signals ($^{139}$La, $^{140}$Ce, $^{141}$Pr, $^{142}$Ce, $^{151}$Eu, $^{153}$Eu) were then normalized to the internal standard ($^{115}$In or $^{197}$Au) and then tested with outlier tests.

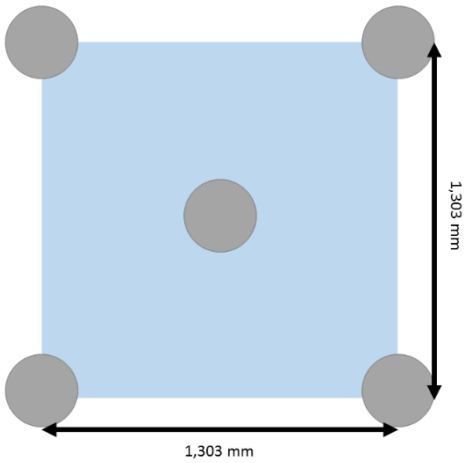


*Figure 14: Schematic drawing of the five-spot-pattern*

The image that was created with the line scan mode had an area of about 317 mm² and the image construction took about 7:15 hours.

*Statistical tests (Pearson and Hartley)*

To generate reliable results a statistic consideration is required. At first it is mandatory to check if the data set correlates a normal distribution. Afterwards the outlier test of Pearson and Hartley was applied.

To identify an outlier a statistic value q has to be calculated with the particular value $x_1$, the average $\bar{x}$ and the standard deviation s (see formula 1).

$$q = \left| \frac{x_1 - \bar{x}}{s} \right|$$

*Formula 1: outlier defied based on the Pearson and Hartley test* [32]

$x_1$ is defined an outlier if q exceeds the critical threshold $q_{crit}$ for a given level of significance α and a sample size (see Table 9).

*Table 9: Statistical $q_{crit}$ for the Pearson and Hartley test*

| Sample Size | $q_{crit}$ (α = 0.01) |
|---|---|
| 25 | 3.351 |
| 50 | 3.539 |

## *d. Immunohistochemistry*

### *i. Sample preparation*

For the immunohistochemistry an optimized staining protocol from abcam was used [33]:

Perform antigen retrieval before commencing with immunostaining if necessary. Reagents were applied manually by pipette and incubations were carried out in Petri plates.

- Wash the slides 2 x 5 min in TBS plus 0.025% Triton X-100 with gentle agitation.
    - *0.025% Triton X-100 in the TBS reduces surface tension, allowing reagents to cover the whole tissue section with ease. It is also believed to dissolve Fc receptors and reduce non-specific binding. We recommend TBS over PBS to get a cleaner background.*

- Block in 10% normal serum with 1% BSA in TBS for 2 h at room temperature.
    - *The secondary antibody may cross react with endogenous immunoglobulins in the tissue. Minimize this by pre-treating the tissue with normal serum from the species in which the secondary was raised.*
    - *The use of normal serum before the application of the primary also eliminates Fc receptor binding of both the primary and secondary antibody. BSA is included to reduce non-specific binding caused by hydrophobic interactions.*

- Drain slides for a few seconds (do not rinse) and wipe around the sections with tissue paper.

- Apply primary antibody diluted in TBS with 1% BSA.
    - *Dilute the primary antibody to the manufacturer's recommendations or to a previously optimized dilution. Most antibodies will be used in IHC-P at a concentration of 0.5–10 µg/mL. The primary antibody should be raised in a species different from the tissue being stained. Eg if you had mouse tissue and your primary antibody was raised in a mouse, an anti-mouse IgG secondary antibody would bind to all the endogenous IgG in the mouse*

*tissue and cause high background. Use of mouse monoclonals on mouse tissue is discussed in our mouse-on-mouse protocol.*

- Incubate overnight at 4°C or 30 min to 2 hours at room temperature
    - *Overnight incubation allows use of antibodies of lower titer or affinity by allowing more time for the antibodies to bind. Regardless of the antibody's titer or affinity for its target, once the tissue has reached saturation point no more binding can take place. Incubate overnight to ensure this occurs.*

- Rinse 2 x 5 min TBS 0.025% Triton with gentle agitation.

For fluorescent detection

- Apply fluorophore-conjugated secondary antibody to the slide diluted in TBS with 1% BSA.
- Incubate for 1 h at room temperature.
    - *These steps should be done in the dark to avoid photobleaching*.
- Rinse 3 x 5 min with TBS.
- Mount using compatible mounting medium and add coverslip.

The use of a fluorescence microscopy offers the highest practical spatial resolution. Besides, it is possible to remove the diffraction limit by using a super resolution microscopy. This enables images with a low nanometric scale. [34]

### *ii. Fluorescence microscopy*

The fluorescence microscopy was done with an Olympus IX71 and a fourfold magnification. To control if the secondary antibody did only bind on tissue 4´,6-diamidino-2-phenylindole (DAPI) was used. It binds strongly to adenine-thymine rich regions in DNA and is used as a fluorescent stain. It has its approximate fluorescence excitation maximum at 358 nm (ultraviolet) and its emission maximum at 461 nm (blue). [35]

### *iii. Chemicals*

*Table 10: Used chemicals*

| Name | Supplier |
|---|---|
| TBS | Sigma Aldrich |
| Triton X-100 | |
| BSA | |
| 10% Normal Goat Serum | Abcam |
| Anti-5HT2A Receptor Antibody | |
| Goat Polyclonal Secondary Antibody to Rabbit IgG-H&L (Alexa Fluor 488) | |

## *e. Metal tagging*

### *i. Preparation*

The metal tagging was done with the labeling kit "Maxpar Antibody Labeling Kit" from Fluidigm [36]. The following protocol from Fluidigm was used to produce the labelled antibodies. This labelling protocol was used because sensitivity as well as the detection limit can be improved comparing to other labelling methods. [37]

0:00 Preload the polymer with lanthanide. 1

1. Spin the polymer tube for 10 seconds in a microfuge to ensure that the reagent is at the bottom of the tube.
2. Resuspend the polymer with 95 µL of L-Buffer.
3. Mix thoroughly by pipetting.
4. Add 5 µL of lanthanide metal solution to the tube (final concentration: 2.5 mM in 100 µL).
5. Mix thoroughly by pipetting.
6. Incubate at 37 °C for 30–40 minutes in a water bath. During incubation, proceed immediately to Step 7 and begin buffer exchange and partial reduction of antibody.

0:30 Perform buffer exchange and partially reduce the antibody

7. Add 100 µg of stock antibody in up to 400 µL R-Buffer to a 50 kDa filter.
8. Centrifuge at 12,000 x g for 10 minutes at room temperature.
9. During centrifugation, dilute 0.5 M TCEP stock to 4 mM in R-Buffer by mixing 8 µL of 0.5 M TCEP stock with 992 µL of R-Buffer. For each antibody being labelled, 100 µL of 4 mM TCEP-R-Buffer is required.
10. Discard column flow-through from centrifugation.
11. Add 100 µL of the 4 mM TCEP-R-Buffer to each antibody and mix by pipetting.
12. Incubate at 37 °C in a water bath for 30 minutes. Proceed to Step 13 during the 30-minute incubation.

IMPORTANT Do not exceed 30 minutes! Proceed immediately to Step 17 after 30 minutes and begin purifying the partially reduced antibody.

0:45 Purify the lanthanide-loaded polymer

NOTE Purify the lanthanide-loaded polymer at the same time that the antibody is being reduced (Step 12)

13. Add 200 µL of L-Buffer to a 3 kDa filter.
14. Add the 100 µL metal-loaded polymer mixture to the filter containing the 200 µL L-Buffer to the wash.
15. Centrifuge at 12,000 x g for 25 minutes at room temperature.
16. Repeat the wash by adding 400 µL of C-Buffer to the filter and centrifuge at 12,000 x g for 30 minutes at room temperature.

1:15 Purify the partially reduced antibody.

17. Retrieve the 50 kDa filter containing the partially reduced antibody from the 37 °C water bath.
18. Add 300 µL of C-Buffer to the 50 kDa filter to wash the antibody.
19. Centrifuge at 12,000 x g for 10 minutes at room temperature.
20. Discard flow-through.
21. Repeat the wash by adding 400 µL of C-Buffer to the filter and centrifuge at 12,000 x g for 10 minutes at room temperature.

1:40 Retrieve the purified partially reduced antibody and lanthanide-loaded polymer

22. Retrieve 3 kDa filter containing the purified lanthanide-loaded polymer from the centrifuge and discard column flow-through.
23. Retrieve 50 kDa filter containing the purified partially reduced antibody from the centrifuge and discard column flow-through.

1:45 Conjugate the antibody with lanthanide-loaded polymer.

24. Using a pipette, resuspend the lanthanide-loaded polymer in 60 µL of C-Buffer (total volume ~80 µL).
25. Transfer the resuspended contents to the corresponding partially reduced antibody in the 50 kDa filter (final conjugation volume ~100 µL).
26. Mix gently by pipetting.
27. Incubate at 37 °C for 90 minutes.

3:15 Wash the metal-conjugated antibody.

28. Add 200 µL of W-Buffer to the 100 µL antibody conjugation mixture.
29. Centrifuge at 12,000 x g for 10 minutes.
30. Discard flow-through.
31. Repeat wash three more times with W-Buffer up to a total volume of 400 µL (for a total of four washes with W-Buffer).

4:20 Recover and store the metal-conjugated antibody.

32. Add the calculated volume of antibody stabilization buffer (120 µL, for about 60% recovery of the antibody) minus the residual volume (~20 µL) to the 50 kDa filter to obtain a final concentration of 0.5 mg/mL of conjugated antibody.
33. Invert the 50 kDa filter over to a new collection tube.
34. Centrifuge the inverted filter/collection tube assembly at 1,000 x g for 2 minutes.
35. Store at 4 °C.

A volume of about 50 µL of the conjugated antibody solution was mixed with antibody stabilization buffer. It is important that the labelled antibody is present in excess and that the interaction with the specimen is enabled for a sufficient time. [38] Hence, the incubation was performed over the weekend at 4°C in order to avoid protein degradation. [37]

# 4. Results and discussion

## *a. Indium and gold as an internal standard*

Since instrumental drifts may occur during the measurement as well as changes in the ablation behavior because of variations in the matrix, it is a requirement to correct the signals of the analytes to the intensity of an internal standard. As discussed previously (2.d) gold is a suitable internal standard for different matrices [39]. Nevertheless, the sputtering process is an additional step. The first experiment was to determine if indium that is already on the ITO-slide is as suitable as gold as an internal standard to facilitate the workflow. Therefore, an experiment with different concentration of REE standards in gelatin with a gold layer on top of it was done.

The following table (Table 11) gives an overview of the generated, not normalized data as relative counts. The standards were measured with the spot scan mode using the pattern of Figure 14 and the parameters of Table 8. Since the spot scan pattern which is constructed of five spots was measured ten times per standard, the average and the standard deviation were calculated with 50 values (n=50). The exception is “Standard 0”, there the pattern was only measured 5 times (n=25). Subsequently, the normalization was accomplished dividing the signal of the standard by the appropriate indium or gold signal following by applying the outlier test from Pearson and Hartley. This edited data is found in the appendix (Appendix-Table 1 – Appendix-Table 4).

*Table 11: In and Au as internal standard: generated data (n=50)*

| STD | $^{139}$La | $^{140}$Ce | $^{141}$Pr | $^{142}$Ce | $^{151}$Eu | $^{153}$Eu | $^{115}$In | $^{197}$Au |
|---|---|---|---|---|---|---|---|---|
| | Counts (a.u.) | | | | | | | |
| 0 | 3.09E03 ± 2.16E02 | 1.69E03 ± 2.27E02 | 4.14E02 ± 6.45E02 | 5.04E02 ± 9.77E01 | 4.49E01 ± 2.73E01 | 3.94E01 ± 2.24E01 | 6.19E06 ± 7.59E05 | 4.37E06 ± 4.96E05 |
| 0.5 | 2.97E03 ± 1.25E03 | 3.38E03 ± 1.27E03 | 2.13E03 ± 1.40E03 | 7.44E02 ± 1.95E02 | 1.00E03 ± 7.50E02 | 1.14E03 ± 8.44E02 | 6.15E06 ± 6.79E05 | 4.79E06 ± 7.44E05 |
| 1 | 5.67E03 ± 6.61E02 | 5.94E03 ± 5.48E02 | 4.97E03 ± 7.64E02 | 1.09E03 ± 1.23E02 | 2.42E03 ± 3.52E02 | 2.69E03 ± 4.14E02 | 5.63E06 ± 2.76E05 | 6.29E06 ± 8.28E05 |
| 2 | 1.12E04 ± 2.54E03 | 1.15E04 ± 2.47E03 | 1.18E04 ± 2.96E03 | 1.82E03 ± 3.36E02 | 6.16E03 ± 1.65E03 | 6.89E03 ± 1.79E03 | 5.95E06 ± 3.26E05 | 7.62E06 ± 2.38E06 |
| 4 | 1.94E04 ± 3.02E03 | 1.92E04 ± 2.82E03 | 2.12E04 ± 3.39E03 | 2.79E03 ± 4.24E02 | 1.06E04 ± 1.74E03 | 1.18E04 ± 1.90E03 | 5.56E06 ± 6.55E05 | 6.31E06 ± 9.64E05 |

It is possible to look at the data in three different ways: they can be normalized to $^{115}$In (a) or $^{197}$Au (b) or they are not normalized (c).

(a) $^{115}$In

The following figure (Figure 15) shows the standards normalized to $^{115}$In and edited with the outlier test. The standard series of $^{141}$Pr is representative for all six REE standards, all the rest can be found in the appendix (Appendix-Figure 1 – Appendix-Figure 3).

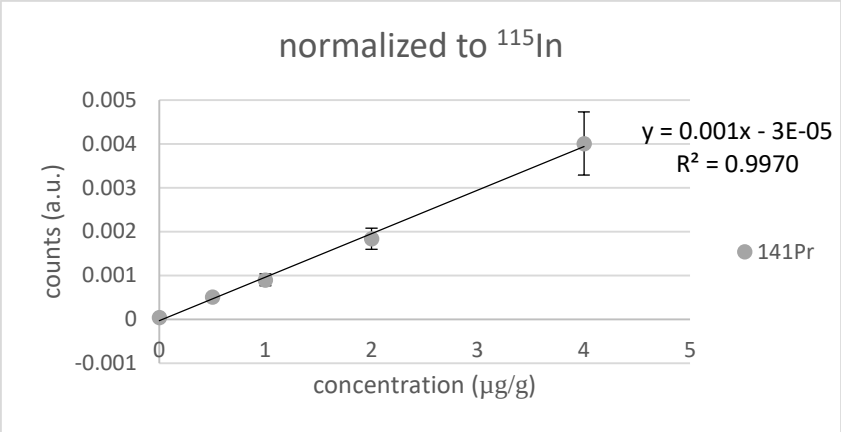


*Figure 15: In and Au as internal standard: standard series for $^{141}$Pr normalized to $^{115}$In*

The following table (Table 12) sums the normalization to $^{115}$In up. There is a linear correlation which reveals a $R^2$ in the range of 0.98-0.99.

*Table 12: Overview of the parameters for the linear equation of the $^{115}$In normalized data*

| | Slope | Intercept | $R^2$ |
|---|---|---|---|
| | Counts (a.u.) | | ( ) |
| $^{139}$La | 0.0008 | + 0.0002 | 0.9981 |
| $^{140}$Ce | 0.0008 | + 0.0003 | 0.9994 |
| $^{141}$Pr | 0.0010 | - 3.00E-05 | 0.9970 |
| $^{142}$Ce | 0.0010 | + 9.00E-05 | 0.9963 |
| $^{151}$Eu | 0.0005 | + 5.00E-06 | 0.9895 |
| $^{153}$Eu | 0.0005 | - 7.00E-06 | 0.9952 |

(b) $^{197}$Au

The following figure (Figure 16) shows the standards normalized to $^{197}$Au and edited with the outlier test. The standard series of $^{14}$1Pr is representative for all six REE standards, all the rest can be found in the appendix (Appendix-Figure 4 – Appendix-Figure 6).

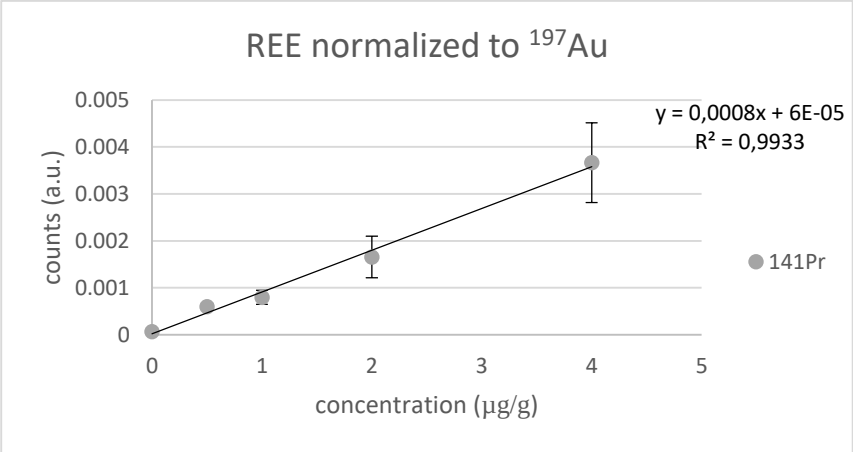


*Figure 16: In and Au as internal standard: standard series for $^{141}$Pr normalized to $^{197}$Au*

The following table (Table 13) sums the normalization to $^{115}$In up. There is a linear correlation which reveals a $R^2$ in the range of 0.97-0.99.

*Table 13: Overview of the parameters for the linear equation of the $^{197}$Au normalized data*

| | Slope | Intercept | $R^2$ |
|---|---|---|---|
| | Counts (a.u.) | | ( ) |
| $^{139}$La | 0.0007 | + 0.0003 | 0.9902 |
| $^{140}$Ce | 0.0007 | + 0.0004 | 0.9909 |
| $^{141}$Pr | 0.0008 | + 6.00E-05 | 0.9933 |
| $^{142}$Ce | 9.00E-05 | + 1.00E-04 | 0.9758 |
| $^{151}$Eu | 0.0004 | + 9.00E-06 | 0.9928 |
| $^{153}$Eu | 0.0005 | + 3.00E-05 | 0.9940 |

(c) Not normalized

The following figure (Figure 17) shows the standards not normalized. The standard series of $^{141}$Pr is representative for all six REE standards, all the rest can be found in the appendix (Appendix-Figure 7 – Appendix-Figure 9).

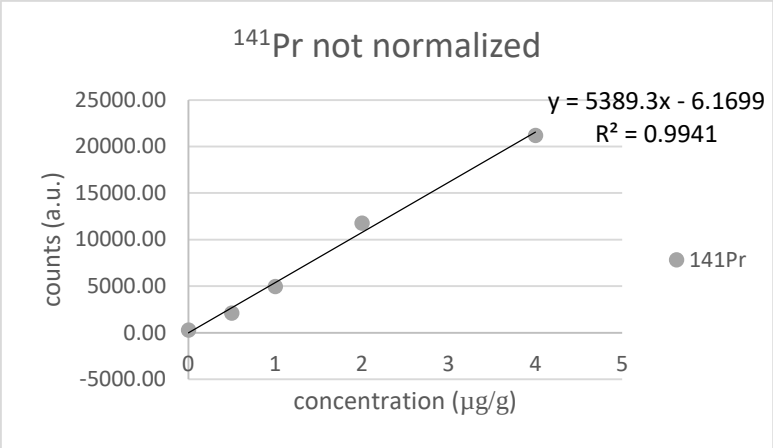


*Figure 17: In and Au as internal standard: standard series for $^{141}$Pr not normalized*

The following table (Table 14) sums the not normalized data up. There is a linear correlation which reveals a $R^2$ in the range of 0.97-0.98.

*Table 14: Overview of the parameters for the linear equation of the $^{197}$Au normalized data*

| | Slope | Intercept | $R^2$ |
|---|---|---|---|
| | Counts (a.u.) | | ( ) |
| $^{139}$La | 3916.2 | + 2225.0 | 0.9761 |
| $^{140}$Ce | 4044.9 | + 1927.4 | 0.9808 |
| $^{141}$Pr | 4888.2 | + 386.5 | 0.9850 |
| $^{142}$Ce | 520.28 | + 557.1 | 0.9752 |
| $^{151}$Eu | 2491.9 | + 117.3 | 0.9765 |
| $^{153}$Eu | 2774.7 | + 137.6 | 0.9759 |

(d) Comparison

A comparison of the relative standard deviation (Table 15) shows that the normalized data leads to a lower RSD than the data that is not normalized. More exactly, the normalization to $^{115}$In results in a lower RSD than the normalization to $^{197}$Au. For example, the $^{141}$Pr normalized to $^{115}$In has RSDs between 7.9% – 17.9% whereas the normalized to $^{197}$Au has RSDs of 10.9% – 26.9%. Altogether the range of the RSD for the not normalized data ranges between 7.0% – 60.1%, between 6.6% – 27.7% for the normalization to $^{115}$In and between 10.1% – 27.7% for the normalization to $^{197}$Au. The "Standard 0" of $^{151}$Eu and $^{153}$Eu

are the only ones that are outside the interval. Common laser ablation experiments provide RSDs of about 10% [39]. One possible reason for the high RSDs of these experiments could be that the used concentrations are low. Another aspect that should be considered is the homogeneity of the used gelatin gels. Šala et al. discovered that the temperate of drying the gelatin gels is a crucial aspect to receive a homogeneous distribution. [17]

*Table 15: Comparison of the relative standard deviation of the data normalized to 115In (red) and 197Au (blue) and the not normalized data*

| Comparison of the relative standard deviation | | | | | | |
|---|---|---|---|---|---|---|
| | $^{139}$La | | | $^{140}$Ce | | |
| STD | Counts (a.u.) | | | | | |
| 0 | 6.6 | 10.6 | 7.0 | 10.1 | 10.1 | 13.5 |
| 0.5 | 8.4 | 25.1 | 42.0 | 8.9 | 22.4 | 37.6 |
| 1 | 10.5 | 16.2 | 11.7 | 10.1 | 16.1 | 9.2 |
| 2 | 13.0 | 24.5 | 22.8 | 9.9 | 27.1 | 21.4 |
| 4 | 19.6 | 23.0 | 35.5 | 23.9 | 27.4 | 35.1 |
| | $^{141}$Pr | | | $^{142}$Ce | | |
| STD | Counts (a.u.) | | | | | |
| 0 | 17.6 | 26.4 | 23.2 | 13.8 | 19.2 | 19.4 |
| 0.5 | 7.9 | 10.9 | 65.7 | 8.1 | 17.1 | 26.3 |
| 1 | 15.0 | 19.1 | 15.4 | 21.6 | 17.9 | 11.3 |
| 2 | 13.0 | 26.9 | 25.1 | 15.0 | 27.6 | 18.4 |
| 4 | 17.9 | 23.2 | 35.7 | 20.3 | 25.4 | 35.4 |
| | $^{151}$Eu | | | $^{153}$Eu | | |
| STD | Counts (a.u.) | | | | | |
| 0 | 49.2 | 49.1 | 60.8 | 44.0 | 43.9 | 56.8 |
| 0.5 | 10.1 | 14.7 | 74.8 | 10.9 | 13.3 | 73.9 |
| 1 | 14.1 | 19.9 | 14.6 | 9.9 | 20.8 | 15.4 |
| 2 | 32.9 | 26.7 | 26.8 | 25.5 | 27.7 | 25.9 |
| 4 | 21.5 | 25.1 | 35.9 | 20.5 | 26.8 | 35.8 |

It is possible to elect $^{115}$In to be the internal standard. On one reason is that the standard deviation is in most cases noticeable lower than for the data that is either normalized to $^{197}$Au or not normalized.
Another aspect is that there is no additional step needed to apply the indium because it is available on the slides. Since there is no sputtering process, it is not possible to carry in contaminations that lead to interferences.

Furthermore, another advantage of the indium is found in the quality of the standard series because there the highest $R^2$ is produced. The $R^2$ has values between 0 – 1 whereas changes below 1 are more significant than above 0 because of its strong non-linearity. The not normalized data lead to $R^2$ between 0.97 – 0.98 whereby a normalization to the $^{115}$In intensity results in $R^2$ between 0.9990 – 0.9994 and the normalization to the $^{197}$Au intensity results in $R^2$ between 0.9758 – 0.9940.

### *b. Quantification with REE Gelatin Standards*

Certified reference material is one of the most reliable methods. Since there is a lack of appropriate materials for imaging experiments which match to a biological origin, gelatin standards were used. In contrast to the previous standard series for the comparison of $^{115}$In and $^{197}$Au as internal standard, another set of standards with an augmented range of concentration was used.

The following tables (Table 16 and Table 17) give an overview of the data normalized to $^{115}$In and edited with the outlier test. The standards were measured with the spot scan mode using the pattern of Figure 14 and the parameters of Table 8. Since the spot scan pattern which is constructed of five spots was measured ten times per standard, the average and the standard deviation were calculated with 50 values (n=50).

*Table 16: Quantification: standard series of REE normalized to $^{115}In$*

| | Normalized to $^{115}In$ | | | | | |
|---|---|---|---|---|---|---|
| | $^{139}La$ | $^{140}Ce$ | $^{141}Pr$ | $^{142}Ce$ | $^{151}Eu$ | $^{153}Eu$ |
| STD | Counts (a.u.) | | | | | |
| 0.3 | 1.83E-04 ± 4.69E-05 | 1.97E-04 ± 1.78E-05 | 7.62E-05 ± 1.92E-05 | 4.58E-05 ± 9.34E-06 | 2.91E-05 ± 1.03E-05 | 2.84E-05 ± 9.79E-06 |
| 0.6 | 2.46E-04 ± 6.79E-05 | 2.48E-04 ± 2.59E-05 | 1.16E-04 ± 3.13E-05 | 5.44E-05 ± 1.19E-05 | 4.49E-05 ± 1.43E-05 | 5.45E-05 ± 1.55E-05 |
| 1.25 | 2.92E-04 ± 8.87E-05 | 3.67E-04 ± 2.83E-05 | 2.25E-04 ± 2.79E-05 | 7.06E-05 ± 1.49E-05 | 1.11E-04 ± 1.54E-05 | 1.18E-04 ± 1.99E-05 |
| 2.5 | 5.43E-04 ± 1.06E-04 | 5.49E-04 ± 7.03E-05 | 4.66E-04 ± 8.70E-05 | 9.77E-05 ± 1.91E-05 | 2.18E-04 ± 3.41E-05 | 2.55E-04 ± 4.94E-05 |
| 5 | 8.09E-04 ± 1.10E-04 | 7.61E-04 ± 7.99E-05 | 7.09E-04 ± 1.02E-04 | 1.28E-04 ± 1.89E-05 | 3.69E-04 ± 5.65E-05 | 4.16E-04 ± 7.04E-05 |
| 9.5 | 1.49E-03 ± 1.40E-04 | 1.48E-03 ± 1.58E-04 | 1.62E-03 ± 1.92E-04 | 2.29E-04 ± 2.93E-05 | 8.86E-04 ± 1.11E-04 | 1.01E-03 ± 1.06E-04 |
| 18 | 3.37E-03 ± 5.29E-04 | 3.25E-03 ± 5.08E-04 | 3.49E-03 ± 5.58E-04 | 4.60E-04 ± 8.23E-05 | 1.82E-03 ± 2.71E-04 | 1.99E-03 ± 3.44E-04 |

*Table 17: Overview of the relative standard deviation generated from the standard series of REE normalized to $^{115}In$*

| | Normalized to $^{115}In$ | | | | | |
|---|---|---|---|---|---|---|
| | $^{139}La$ | $^{140}Ce$ | $^{141}Pr$ | $^{142}Ce$ | $^{151}Eu$ | $^{153}Eu$ |
| STD | Counts (a.u.) | | | | | |
| 0.3 | 25.7 | 9.0 | 25.2 | 20.4 | 35.5 | 34.4 |
| 0.6 | 27.6 | 10.4 | 26.9 | 21.9 | 31.9 | 28.4 |
| 1.25 | 30.4 | 7.7 | 12.4 | 21.1 | 13.9 | 16.9 |
| 2.5 | 19.6 | 12.8 | 18.7 | 19.6 | 15.7 | 19.4 |
| 5 | 13.5 | 10.5 | 14.4 | 14.8 | 15.3 | 16.9 |
| 9.5 | 9.4 | 10.6 | 11.9 | 12.8 | 12.6 | 10.6 |
| 18 | 15.7 | 15.6 | 16.0 | 17.9 | 14.9 | 17.3 |

The following figure (Figure 18) shows the standard series of $^{141}Pr$ which is representative for all six REE standards, all the rest can be found in the appendix (Appendix-Figure 10 – Appendix-Figure 12).

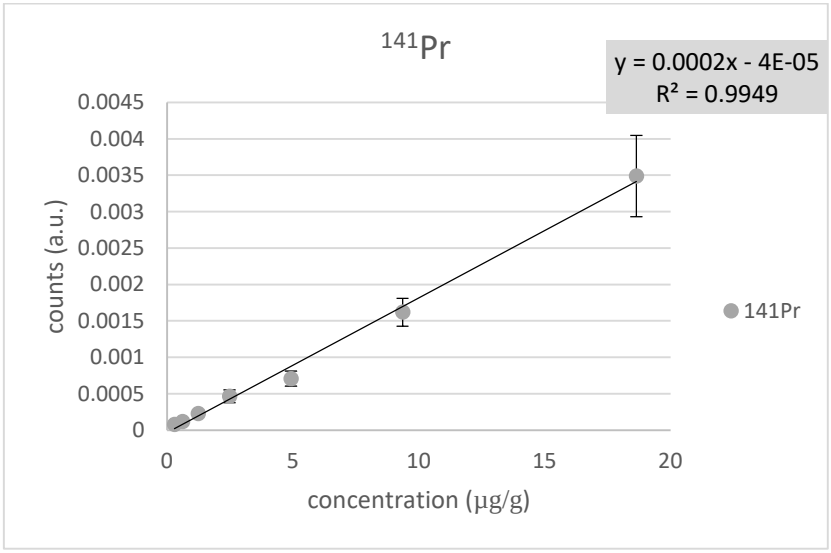


*Figure 18: Quantification: standard series of $^{141}Pr$*

The following table (Table 18) sums data up. There is a linear correlation which reveals a $R^2$ in the range of 0.9911-0.9969.

*Table 18: Overview of the parameters for the linear equation of the data for the quantification experiment*

| | Slope | Intercept | $R^2$ |
|---|---|---|---|
| | Counts (a.u.) | | ( ) |
| $^{139}La$ | 0.0002 | + 7.00E-05 | 0.9916 |
| $^{140}Ce$ | 0.0002 | + 0.0001 | 0.9911 |
| $^{141}Pr$ | 0.0002 | - 4.00E-05 | 0.9949 |
| $^{142}Ce$ | 2.00E-05 | + 4.00E-05 | 0.9943 |
| $^{151}Eu$ | 1.00E-04 | - 3.00E-05 | 0.9965 |
| $^{153}Eu$ | 0.0001 | - 2.00E-05 | 0.9969 |

To sum Table 17 up, the relative standard deviations are mainly between the interval of 7.7% – 28.4%. There are only a few standards that have a relative standard deviation above 30% (Standard 1.25 $^{139}La$, standard 0.6 $^{151}Eu$ and standard 0.3 $^{153}Eu$). This trend is

similar to the data from chapter 4.a. As mention before, common laser ablation experiments provide RSDs of about 10% [39]. A possible reason for the high RSDs could be found in the inhomogeneity of the gelatin. It should also be mentioned that the $R^2$ for all REE is above 0.99.

Limit of Detection

There is a limit of where a sample is significantly distinguishable from the blank. This limit of detection is the chance that a blank is identified as sample through an error. Typically, the chance is of five percent (α=0.05). It is calculated by adding the doubled standard deviation s to the average $\bar{x}$ (see formula 2).

$$LOD = \bar{x} + 2 \cdot s$$

*Formula 2: Limit of Detection* [32]

Table 19 summarizes the calculated limit of detections.

*Table 19: Limit of Detection*

| | $^{139}$La | $^{140}$Ce | $^{141}$Pr | $^{142}$Ce | $^{151}$Eu | $^{153}$Eu |
|---|---|---|---|---|---|---|
| $\bar{x}$ | 1.98E-04 | 2.68E-04 | 4.56E-05 | 8.12E-05 | 8.58E-06 | 6.60E-06 |
| s | 1.31E-05 | 2.70E-05 | 8.03E-06 | 1.12E-05 | 4.22E-06 | 2.90E-06 |
| LOD | 2.24E-04 | 3.22E-04 | 6.17E-05 | 1.04E-04 | 1.70E-05 | 1.24E-05 |

### *c. Receptor detection*

The conjugated antibody was applied as discussed in chapter 3.e. After the incubation was stopped, the sample was washed with deionized water and was measured with LA-ICP-MS, using the line scan mode with the parameters of Table 8.

Since the image that was created had an area of approximately 317 mm², the image construction took about 7:15 h.

Figure 19 shows pictures of the brain tissue before (left) and after (right) applying the antibody solution. Although the sample was washed with deionized water it is still identifiable where the antibody – buffer solution was applied. It is as well visible that there is an erosion of the tissue.

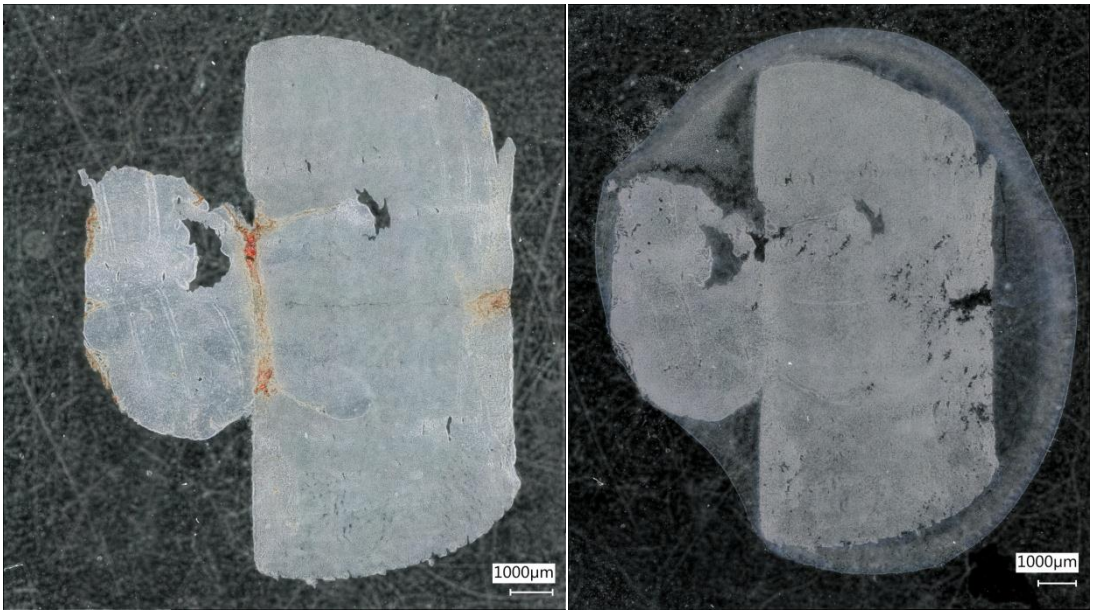


*Figure 19: Brain tissue before (left) and after (right) applying the antibody solution*

After the measurement the data was imported into ImageLab (Version 2.96) and the images were created. The following figures show the resulting distribution of the elements $^{13}C$ (Figure 20) and $^{141}Pr$ (Figure 21).

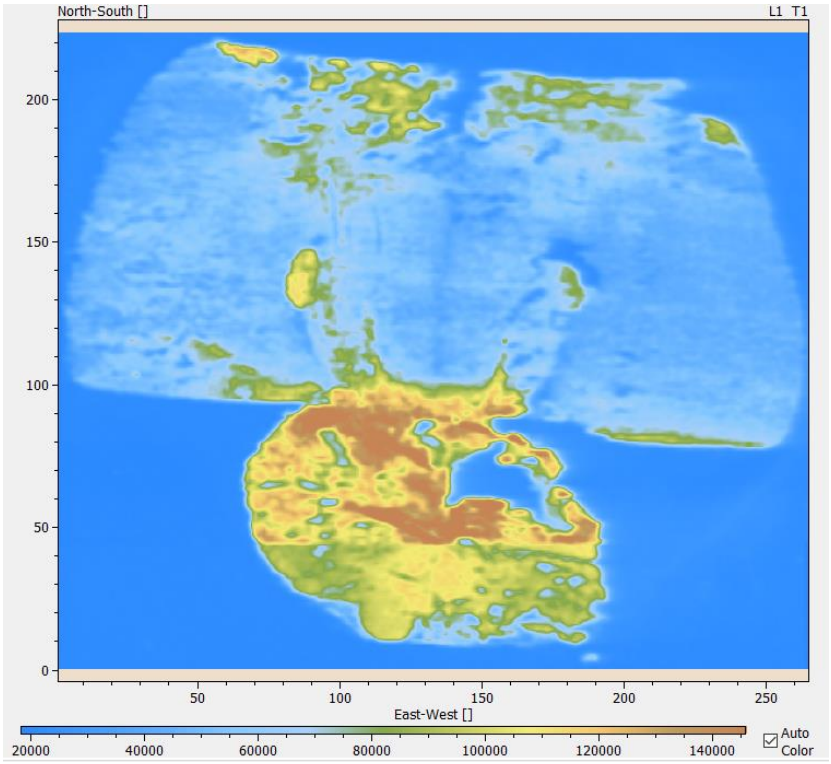


*Figure 20: Distribution of $^{13}C$ (tissue: rat brain)*

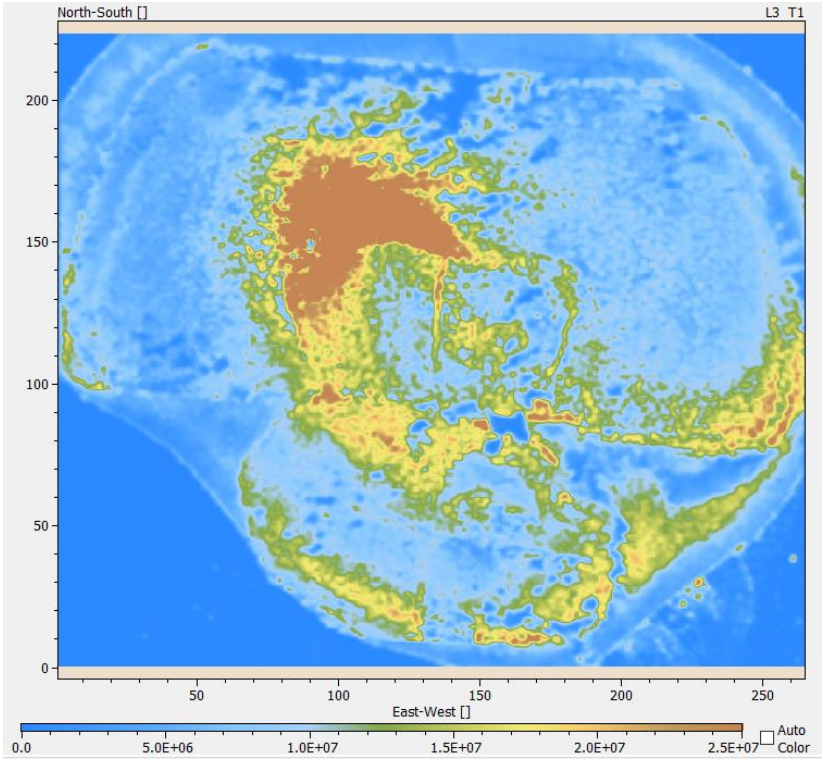


*Figure 21: Distribution of $^{141}Pr$ (tissue: rat brain)*

The distribution of $^{13}C$ should be evenly but the signal intensity varies between 6000 (correlates to the color light blue) until 14000 counts (correlates to the color brown). Still, this distribution helps to define the scope and area of the tissue.

The distribution of $^{141}Pr$ is correlated to the distribution of the 5HT2A receptor. Due to the distribution in the image, it can be said that the 5HT2A receptor is not evenly distributed within the rat brain. There are locations where it is rarely present (in Figure 21 represented trough the color light blue) and where it is densely located (represented through the color brown). It is striking that Praseodymium is outside the sample present. Perhaps the incubation was too long.

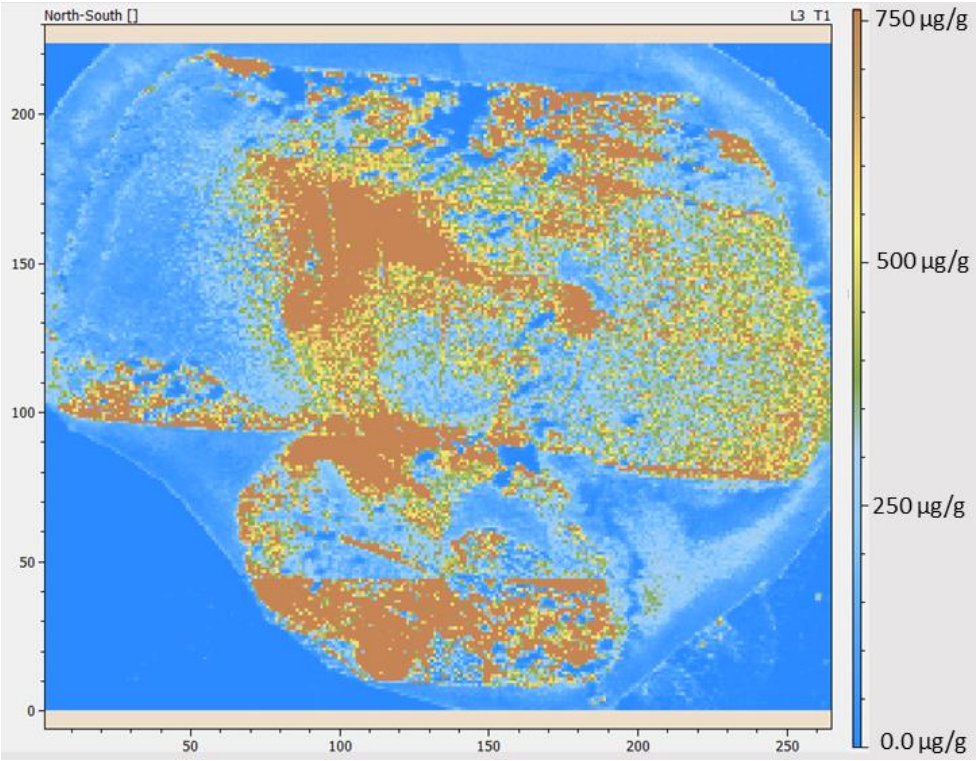


*Figure 22: Quantification of $^{141}Pr$ (tissue: rat brain)*

Quantification of the derived signal was based on the calibration of the gelatin standards. Figure 22 shows the normalized signal to the internal standard $^{115}In$. The concentration ranges between 0-750- $\mu g g^{-1}$. Normally the intensity plot offers only information about the qualitative distribution. Anyway, it was possible to gain quantitative information about the distribution of $^{141}Pr$. Notwithstanding, it should be mentioned, that the Waentig et al. used a SDS-PAGEG gel to characterize the antibodies after denaturation and by calculating the

labeling degree. The antibodies were generally separated into the heavy and light chains. The exceptions were antibodies labelled with the labeling kit from Fluidigm. They showed weak and broad bands that lead to the two hypotheses that the polymer tag reagent contains molecules with different lengths, resulting in definitely not sharp distribution of molecular weight and that the antibodies are eventually modified with different numbers of labels. They concluded that with these considerations, it might cause difficulties in quantification. [40]

Actually, it was planned to compare the distribution of the receptor generated by the immunohistochemical detection to the image generated by LA-ICP-MS. Nevertheless, it was not possible to create an informative image by the fluorescence microscope. The staining protocol was probably too aggressive for the tissue because afterwards some parts were ablated and the scope of the origin sample was not recognizable. However, there was an area that could be assigned by comparing with the other tissue sections.

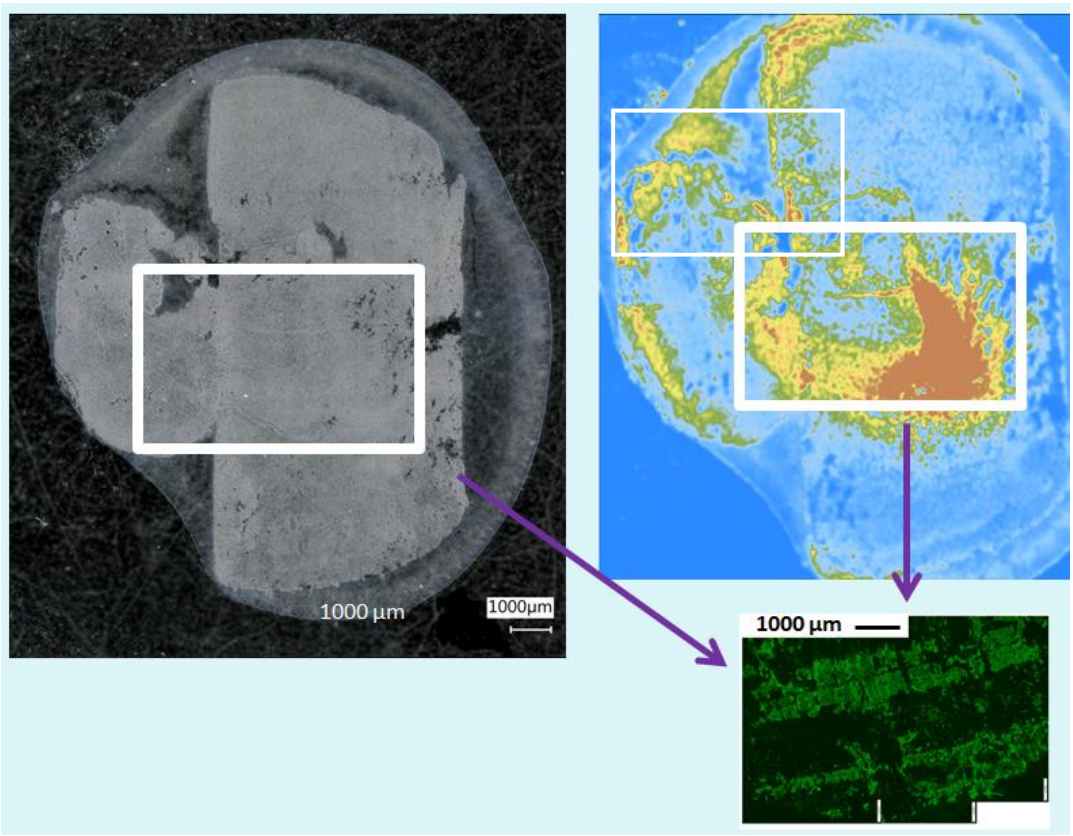


*Figure 23: Comparison of the distribution of the 5-HT2A receptor*

Figure 23 shows a comparison of the created distributions of the 5-HT2A receptor. It is only an assumption that the regions fit because similarities between the microscope pictures were searched. Both images show that the distribution of the 5-HT2A receptor is not consistent and that there are regions with a higher and regions with a lower or no concentration.

# 5. Conclusion and Outlook

Information about the distribution of elements helps to understand different processes and to gain fundamental information. Since medical diseases like depression affects more and more people, information that helps the curing process are of special interest. The family of 5-HT receptor plays an important role because the effect of antidepressants can be enhanced by their modulation. The 5-HT2A receptor was chosen as an example. Inasmuch as it is located nearly in the whole central nervous system, it was possible to used brain tissues as samples. The common method of illustrating the distribution is with immunohistochemistry. A suitable antibody binds specifically to the analyte receptor. For visualization there are many possibilities. However, this step is the limiting one. Therefore, only a sector of receptors is presentable. Certainly, it is possible to detect the 5-HT2A receptor. In this work a secondary antibody was used that was conjugated to a fluorophore and has a high specificity to bind to the primary antibody.

The alternative method that extends the range is laser ablation inductively coupled plasma mass spectrometry (LA-ICP-MS). The topic and aim of this research is to examine, if this assumption is viable and to generate a workflow. Since there are some challenges with this method, they have to be regarded as well as compensated.

During the measurement wit LA-ICP-MS, instrumental drifts and matrix effects due to the inhomogeneity of biological samples can occur. These effects lead to changes in the signal intensity. Since the ablation is not similar for all kind of samples, standards have to be used to get a trustworthy quantitative determination of the composition of the sample. There are different kinds of approaches. Gelatin gels were chosen because they imitate animal material like the used brain and are easy in handling. As standards the rare earth elements lanthanum, cerium, praseodymium and europium were used because they have no or less isobaric interferences. The standard were prepared in concentrations between 0.3 – 18.5 µg/g (a detailed listing is given in table 20) and measured simultaneously with the spot scan and a special pattern (Figure 14) that led to 50 values per rare earth element and standard.

*Table 20: Concentration of the REE Gelatin Standards for quantification*

| La (µg/g) | Ce (µg/g) | Pr (µg/g) | Eu (µg/g) |
|---|---|---|---|
| 0.299 | 0.300 | 0.299 | 0.302 |
| 0.613 | 0.615 | 0.612 | 0.620 |
| 1.240 | 1.244 | 1.238 | 1.253 |
| 2.482 | 2.491 | 2.479 | 2.510 |
| 4.929 | 4.946 | 4.924 | 4.984 |
| 9.365 | 9.399 | 9.356 | 9.470 |
| 18.663 | 18.730 | 18.645 | 18.873 |

The generated data led to relative standard deviations (RSD) in the interval of mainly 7.7% – 28.4%. Unfortunately, common laser ablation experiments provide RSDs of about 10% [39]. Perhaps the problem could be found in the homogeneity of the gelatine gels. It is essential to choose the right temperature of drying the gels. In this work room temperature was used. Maybe a higher temperature (100°C) improves the data. Šala et al. showed that room temperature leads to a non-optimal distribution of the standard ions. In comparison, a higher temperature offers a better homogeneity. [17] Nevertheless, the standard series offered a strong linearity with $R^2$ of above 0.99. Additionally, it was possible to calculate the limit of detection (LOD). This data is resumed in Table 21. To show the effect of normalization, the data was also edited using no internal standard. The results showed that normalization offers improved data.

*Table 21: Limit of Detection*

| | $^{139}$La | $^{140}$Ce | $^{141}$Pr | $^{142}$Ce | $^{151}$Eu | $^{153}$Eu |
|---|---|---|---|---|---|---|
| LOD | 2.24E-04 | 3.22E-04 | 6.17E-05 | 1.04E-04 | 1.70E-05 | 1.24E-05 |

It should be mentioned that there are still physical and chemical differences between sample and standard. This has to be corrected by an internal standard. This internal standard should also compensate the aforementioned instrumental drifts.

It was necessary to choose an appropriate internal standard. One opportunity was the often used gold that is applied by sputtering a homogenous layer on top of the sample. However, there was an alternative: sample slides that contained a thin layer of an indium-tin-oxide. The indium of the layer was also a possible candidate. Therefore, it was tested which of these two elements is more suitable. The experiments showed that indium provided not only a better reproducibility with higher relative standard deviations but also a better quality of the linear equation with higher $R^2$ (Overview in Table 22). Supplementary, the workflow was facilitated because no additional sputtering process is needed.

*Table 22: Overview of RSD and $R^2$ of the experiments for the internal standard*

| | Normalized to $^{115}In$ | Normalized to $^{197}Au$ |
|---|---|---|
| RSD (%) | 7.9 – 17.9 | 6.6 – 27.7 |
| $R^2$ (-) | 0.9990 – 0.9994 | 0.9758 – 0.9940 |

The next step was to generate the distribution of the 5HT2A receptor with LA-ICP-MS. For this reason, the antibody had first been tagged to the rare earth element praseodymium. This element is not naturally occurring in biological samples. Hence, it is possible to unambiguously detect the receptor.

At first, the antibody was labelled with a labeling kit. Afterwards the sample was measured with LA-ICP-MS using the line scan. The sample had an area of approximately 317 $mm^2$ and the image construction took about 7:15 h. The generated image showed that the distribution of the receptor is not consistent. There are regions with a higher and regions with a lower concentration. Finally, it was also possible to get quantitative information. Therefore the standard series of praseodymium from the aforementioned quantification experiment was used. Another aspect was to compare this image with the result from the immunohistochemistry. Admittedly, it was difficult. Sadly, it is not possible to use the same tissue section for both analyses.

To improve the comparison there are several approaches. One opportunity is to take similar tissue sections. Although the used samples were cut consecutive, they looked different under the light microscope. It additionally seems that the tissue was highly

strained during the staining protocol. Maybe it is more sensible to use another fixation, for example paraffin-embedded tissues or to quit the secondary antibody with the fluorophore and use a labelled primary antibody. However, it is not guaranteed that the concentration of the receptor is high enough and that there is a labelled primary antibody available.

In addition, it should be tested if the distribution of other receptors is representable with LA-ICP-MS and if it is possible to create an image with the distribution of more receptors at a single experiment. If the used parameters are suitable this would lead to the advantage that there is only one image creation.

# Appendix

*Appendix-Table 1: In and Au as internal standard: standards normalized to $^{115}$In and edited with the outlier test*

| | Normalized to $^{115}$In | | | | | |
|---|---|---|---|---|---|---|
| | $^{139}$La | $^{140}$Ce | $^{141}$Pr | $^{142}$Ce | $^{151}$Eu | $^{153}$Eu |
| STD | Counts (a.u.) | | | | | |
| 0 | 1.98E-04 ± 1.31E-05 | 2.68E-04 ± 2.70E-05 | 4.56E-05 ± 8.03E-06 | 8.12E-05 ± 1.12E-05 | 8.58E-06 ± 4.22E-06 | 6.60E-06 ± 2.90E-06 |
| 0.5 | 6.43E-04 ± 5.41E-05 | 7.24E-04 ± 6.46E-05 | 5.07E-04 ± 4.00E-05 | 1.43E-04 ± 1.16E-05 | 2.44E-04 ± 2.46E-05 | 2.91E-04 ± 3.18E-05 |
| 1 | 1.02E-03 ± 1.07E-04 | 1.05E-03 ± 1.06E-04 | 8.98E-04 ± 1.35E-04 | 2.11E-04 ± 4.57E-05 | 4.24E-04 ± 5.96E-05 | 4.48E-04 ± 4.44E-05 |
| 2 | 1.76E-03 ± 2.28E-04 | 1.81E-03 ± 1.78E-04 | 1.84E-03 ± 2.39E-04 | 3.02E-04 ± 4.51E-05 | 1.14E-03 ± 3.74E-04 | 1.16E-03 ± 2.96E-04 |
| 4 | 3.57E-03 ± 7.00E-04 | 3.39E-03 ± 8.11E-04 | 4.01E-03 ± 7.17E-04 | 5.02E-04 ± 1.02E-04 | 1.96E-03 ± 4.20E-04 | 2.17E-03 ± 4.45E-04 |

*Appendix-Table 2: In and Au as internal standard: relative standard deviation of the data normalized to $^{115}$In and edited with the outlier test*

| | Normalized to $^{115}$In | | | | | |
|---|---|---|---|---|---|---|
| | $^{139}$La | $^{140}$Ce | $^{141}$Pr | $^{142}$Ce | $^{151}$Eu | $^{153}$Eu |
| STD | Counts (a.u.) | | | | | |
| 0 | 6.6 | 10.1 | 17.6 | 13.8 | 49.2 | 44.0 |
| 0.5 | 8.4 | 8.9 | 7.9 | 8.1 | 10.1 | 10.9 |
| 1 | 10.5 | 10.1 | 15.0 | 21.6 | 14.1 | 9.9 |
| 2 | 13.0 | 9.9 | 13.0 | 15.0 | 32.9 | 25.5 |
| 4 | 19.6 | 23.9 | 17.9 | 20.3 | 21.5 | 20.5 |

*Appendix-Table 3: In and Au as internal standard: standards normalized to $^{197}$Au and edited with the outlier test*

| | Normalized to $^{197}$Au | | | | | |
|---|---|---|---|---|---|---|
| | $^{139}$La | $^{140}$Ce | $^{141}$Pr | $^{142}$Ce | $^{151}$Eu | $^{153}$Eu |
| STD | Counts (a.u.) | | | | | |
| 0 | 2.85E-04 ± 3.64E-05 | 3.96E-04 ± 4.32E-05 | 6.42E-05 ± 1.69E-05 | 1.18E-04 ± 2.26E-05 | 1.22E-05 ± 6.01E-06 | 9.31E-06 ± 4.09E-06 |
| 0.5 | 7.43E-04 ± 1.73E-04 | 8.10E-04 ± 1.81E-04 | 6.27E-04 ± 9.56E-05 | 1.71E-04 ± 2.89E-05 | 3.08E-04 ± 5.93E-05 | 3.49E-04 ± 5.26E-05 |
| 1 | 9.68E-04 ± 1.57E-04 | 9.54E-04 ± 1.53E-04 | 7.97E-04 ± 1.52E-04 | 1.76E-04 ± 3.14E-05 | 3.92E-04 ± 7.79E-05 | 4.36E-04 ± 9.05E-05 |
| 2 | 1.56E-03 ± 3.82E-04 | 1.59E-03 ± 3.96E-04 | 1.63E-03 ± 4.13E-04 | 2.52E-04 ± 6.46E-05 | 8.65E-04 ± 2.16E-04 | 9.41E-04 ± 2.40E-04 |
| 4 | 3.43E-03 ± 7.87E-04 | 3.12E-03 ± 8.53E-04 | 3.66E-03 ± 8.49E-04 | 4.68E-04 ± 1.19E-04 | 1.80E-03 ± 4.52E-04 | 1.96E-03 ± 5.25E-04 |

*Appendix-Table 4: In and Au as internal standard: relative standard deviation of the data normalized to $^{115}$In and edited with the outlier test*

| | Normalized to $^{197}$Au | | | | | |
|---|---|---|---|---|---|---|
| | $^{139}$La | $^{140}$Ce | $^{141}$Pr | $^{142}$Ce | $^{151}$Eu | $^{153}$Eu |
| STD | Counts (a.u.) | | | | | |
| 0 | 10.6 | 10.1 | 26.4 | 19.2 | 49.1 | 43.9 |
| 0.5 | 25.1 | 22.4 | 10.9 | 17.1 | 14.7 | 13.3 |
| 1 | 16.2 | 16.1 | 19.1 | 17.9 | 19.9 | 20.8 |
| 2 | 24.5 | 27.1 | 26.9 | 27.6 | 26.7 | 27.7 |
| 4 | 23.0 | 27.4 | 23.2 | 25.4 | 25.1 | 26.8 |

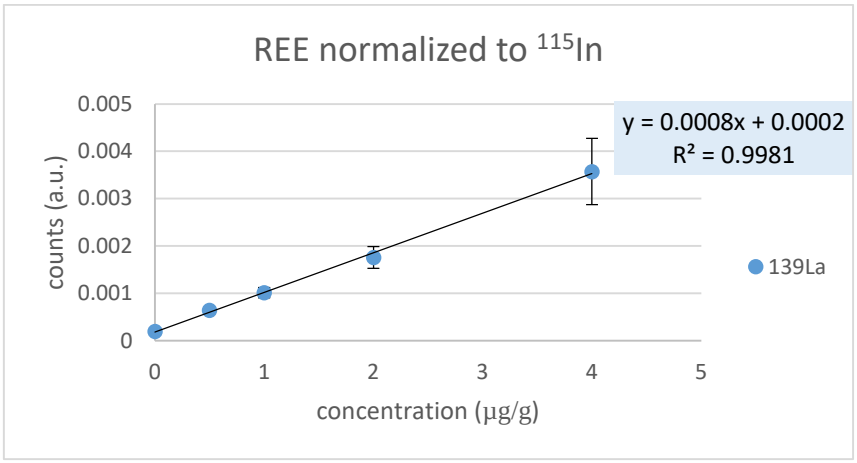


*Appendix-Figure 1: In and Au as internal standard: standard series for $^{139}La$ normalized to $^{115}In$*

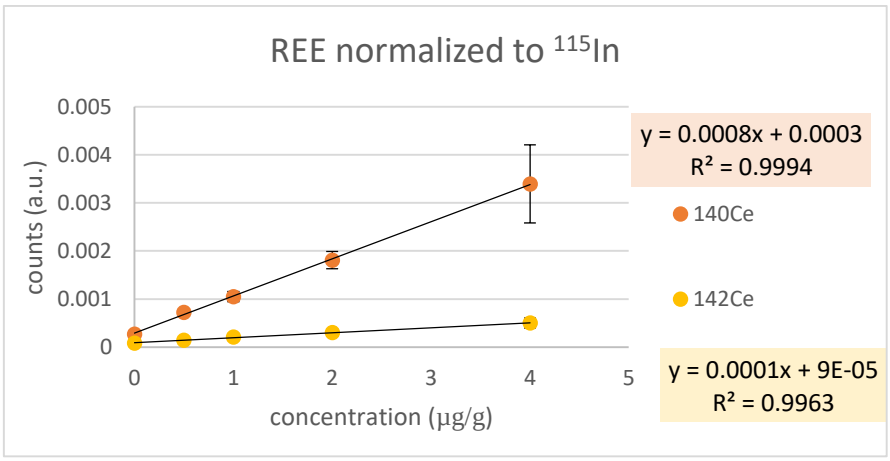


*Appendix-Figure 2: In and Au as internal standard: standard series for $^{140}Ce$ (orange) and $^{142}Ce$ (yellow) normalized to $^{115}In$*

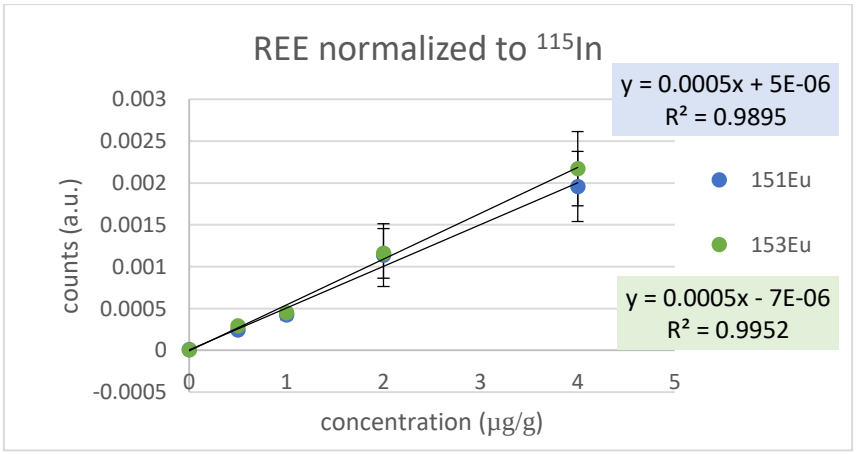


*Appendix-Figure 3: In and Au as internal standard: standard series for $^{151}Eu$ (blue) and $^{153}Eu$ (green) normalized to $^{115}In$*

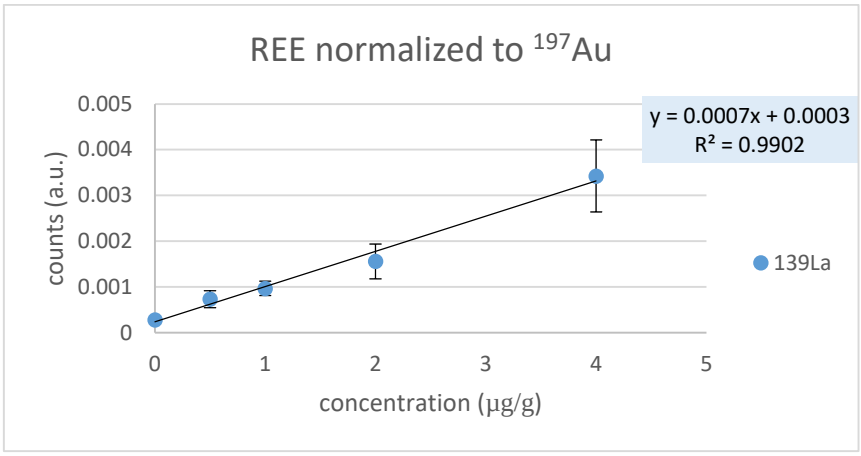


*Appendix-Figure 4: In and Au as internal standard: standard series for $^{139}$La normalized to $^{197}$Au*

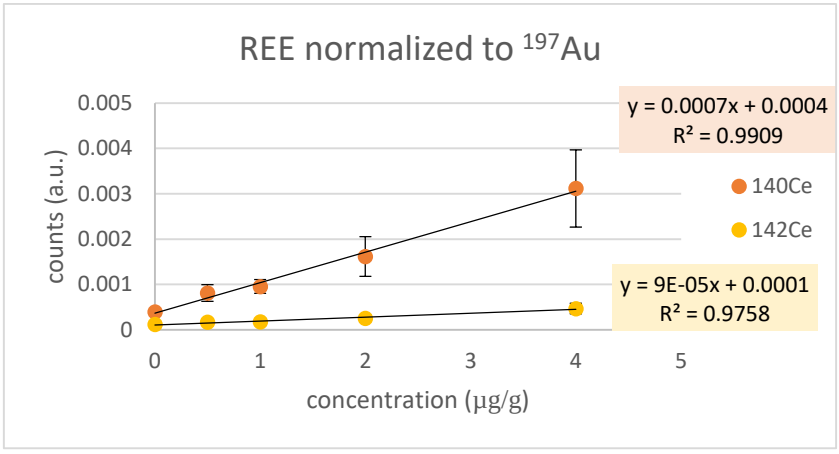


*Appendix-Figure 5: In and Au as internal standard: standard series for $^{140}$Ce (orange) and $^{142}$Ce (yellow) normalized to $^{197}$Au*

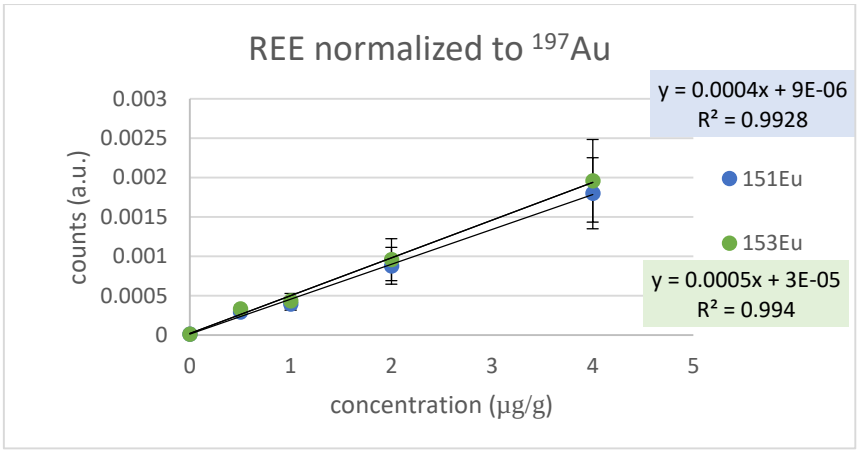


*Appendix-Figure 6: In and Au as internal standard: standard series for $^{151}$Eu (blue) and $^{153}$Eu (green) normalized to $^{197}$Au*

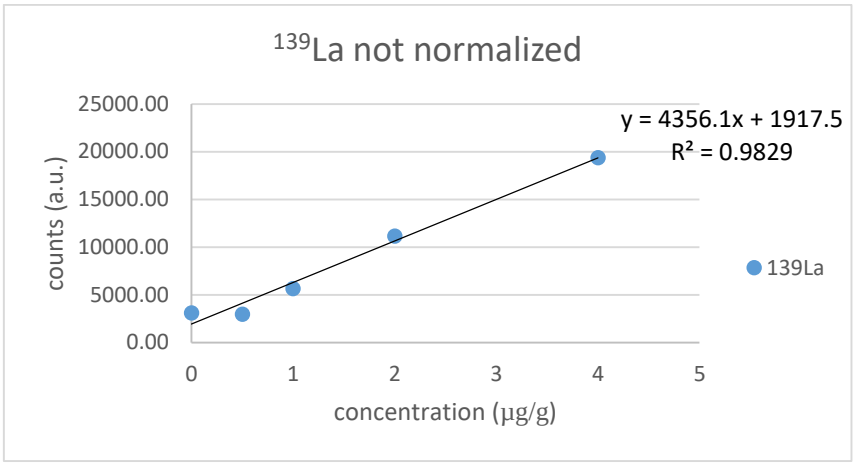


*Appendix-Figure 7: In and Au as internal standard: standard series for $^{139}$La not normalized*

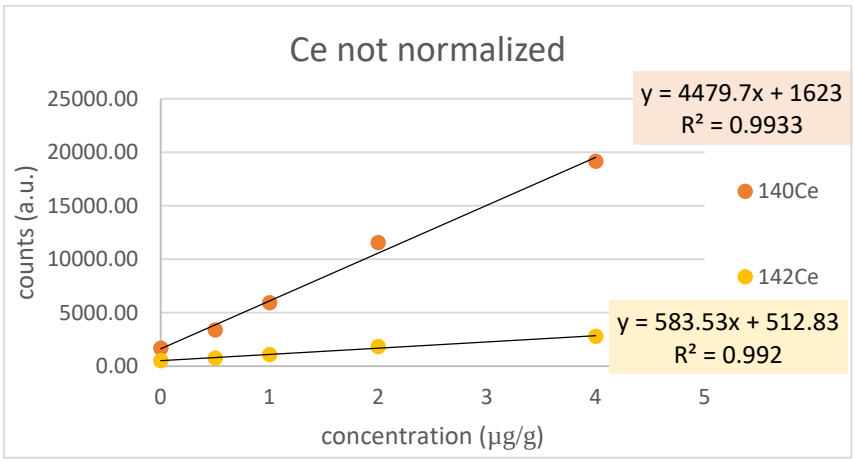


*Appendix-Figure 8: In and Au as internal standard: standard series for $^{140}$Ce and $^{142}$Ce not normalized*

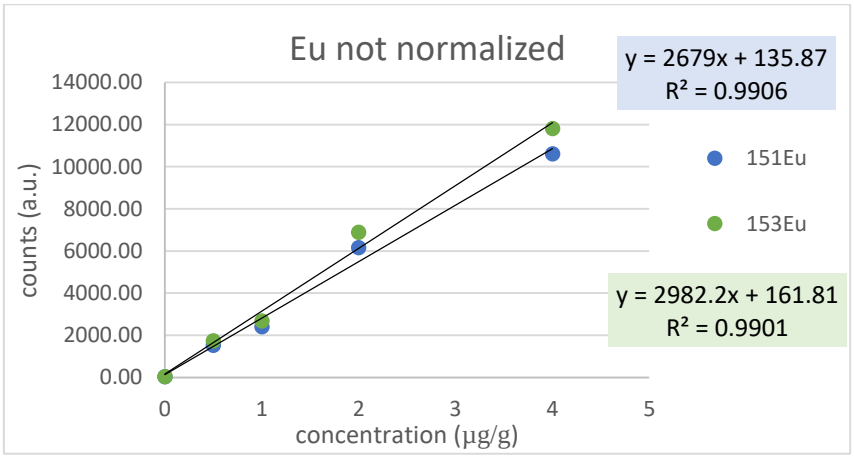


*Appendix-Figure 9: In and Au as internal standard: standard series for 151Eu and 153Eu not normalized*

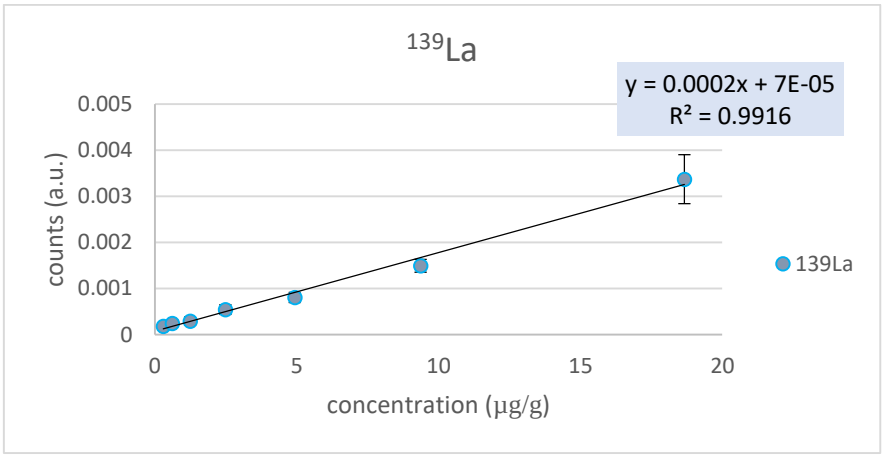


*Appendix-Figure 10: Quantification: standard series of $^{139}La$*

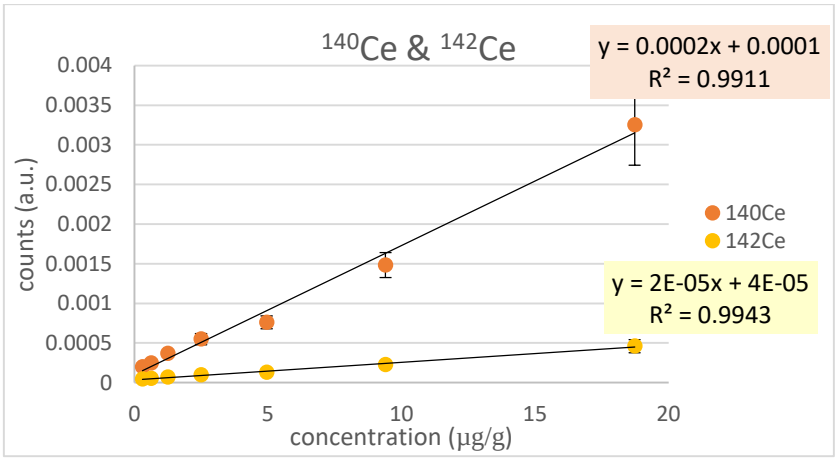


*Appendix-Figure 11: Quantification: standard series of $^{140}Ce$ and $^{142}Ce$*

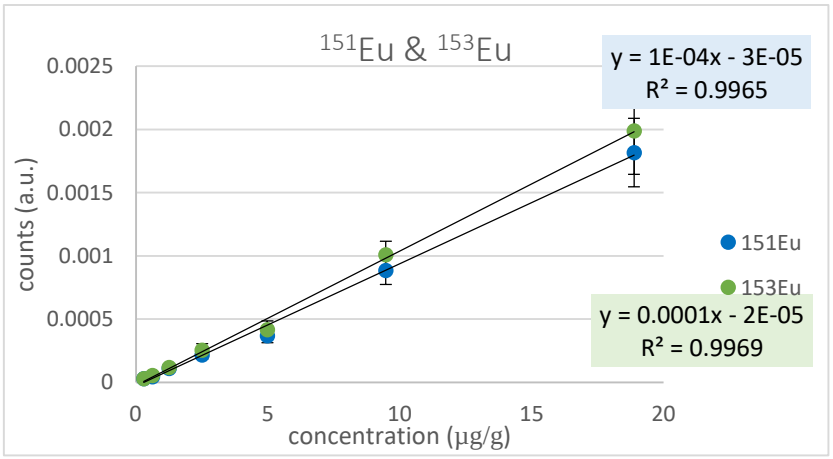


*Appendix-Figure 12: Quantification: standard series of $^{151}Eu$ and $^{153}Eu$*

# Figures

Figure 1: Schematics of an inductively coupled plasma mass spectrometer (ICP-MS) [10] ..... 5
Figure 2: Schematic of a nebulizer [11] ..... 6
Figure 3: ICP left: concentric quartz tubes [3] right: schematic diagram [12] ..... 7
Figure 4: ICP MS vacuum interface [13] ..... 8
Figure 5: Overview of a Quadrupole MS [14] ..... 9
Figure 6: Schematic of a laser ablation unit [15] ..... 11
Figure 7: Schematics of a line scan pattern (left) and a spot scan pattern (right) ..... 13
Figure 8: Software generated diagramm ..... 14
Figure 9: Overview of the metal tagging process [19] ..... 16
Figure 10: Basic principle of an IHC-assay [26] ..... 19
Figure 11: Thermo Scientific iCAP Q ICP-MS used for the experiments [29] ..... 23
Figure 12: ESI NWR 213 used for the experiments [30] ..... 24
Figure 13: Thermo Scientific CryoStar NX50 [31] ..... 25
Figure 14: Schematic drawing of the five-spot-pattern ..... 28
Figure 15: In and Au as internal standard: standard series for $^{141}$Pr normalized to $^{115}$In ..... 37
Figure 16: In and Au as internal standard: standard series for $^{141}$Pr normalized to $^{197}$Au ..... 38
Figure 17: In and Au as internal standard: standard series for $^{141}$Pr not normalized ..... 39
Figure 18: Quantification: standard series of $^{141}$Pr ..... 43
Figure 19: Brain tissue before (left) and after (right) applying the antibody solution ..... 45
Figure 20: Distribution of $^{13}$C (tissue: rat brain) ..... 46
Figure 21: Distribution of $^{141}$Pr (tissue: rat brain) ..... 46
Figure 22: Quantification of $^{141}$Pr (tissue: rat brain) ..... 47
Figure 23: Comparison of the distribution of the 5-HT2A receptor ..... 48

# Tables

Table 1 Characteristics of the used Rare Earth Elements (REE) ..... 16
Table 2: Chemicals used for the preparation of the gelatin standards ..... 21
Table 3: Chemicals of the labeling kit from Fluidigm ..... 22
Table 4: Parameters of the ICP-MS measurements ..... 23
Table 5: Parameters for the laser ablation for the NIST-measurements ..... 24
Table 6: Concentration of the REE gelatin standards for the comparison of the internal standards ..... 26
Table 7: Concentration of the REE Gelatin Standards for quantification ..... 26
Table 8: Parameters for the LA-ICP-MS experiments ..... 27
Table 9: Statistical $q_{crit}$ for the Pearson and Hartley test ..... 28
Table 10: Used chemicals ..... 31
Table 11: In and Au as internal standard: generated data (n=50) ..... 36
Table 12: Overview of the parameters for the linear equation of the $^{115}$In normalized data ..... 37
Table 13: Overview of the parameters for the linear equation of the $^{197}$Au normalized data ..... 38
Table 14: Overview of the parameters for the linear equation of the $^{197}$Au normalized data ..... 39
Table 15: Comparison of the relative standard deviation of the data normalized to 115In (red) and 197Au (blue) and the not normalized data ..... 40
Table 16: Quantification: standard series of REE normalized to $^{115}$In ..... 42

Table 17: Overview of the relative standard deviation generated from the standard series of REE normalized to $^{115}$In ..... 42
Table 18: Overview of the parameters for the linear equation of the data for the quantification experiment ..... 43
Table 19: Limit of Detection ..... 44
Table 20: Concentration of the REE Gelatin Standards for quantification ..... 51
Table 21: Limit of Detection ..... 51
Table 22: Overview of RSD and $R^2$ of the experiments for the internal standard ..... 52
Table 23: REE normalized to Au (Data edited with outlier test) ..... **Fehler! Textmarke nicht definiert.**

# Literature

[1] R&D Systems: Bio-Techne Brand, "IHC / ICC Protocol Guide," 2014.

[2] M. M. Bolognesi *et al.*, "Multiplex Staining by Sequential Immunostaining and Antibody Removal on Routine Tissue Sections," *J. Histochem. Cytochem.*, vol. 65, no. 8, pp. 431–444, 2017.

[3] S. Kirkeby and C. E. Thomsen, "Quantitative immunohistochemistry of fluorescence labelled probes using low-cost software," *J. Immunol. Methods*, vol. 301, no. 1–2, pp. 102–113, 2005.

[4] I. Konz *et al.*, "Gold internal standard correction for elemental imaging of soft tissue sections by LA-ICP-MS: Element distribution in eye microstructures," *Anal. Bioanal. Chem.*, vol. 405, no. 10, pp. 3091–3096, 2013.

[5] C. Austin, D. Hare, T. Rawling, A. M. McDonagh, and P. Doble, "Quantification method for elemental bio-imaging by LA-ICP-MS using metal spiked PMMA films," *J. Anal. At. Spectrom.*, vol. 25, no. 5, pp. 722–725, 2010.

[6] F. Calderón-Celis, J. R. Encinar, and A. Sanz-Medel, "Standardization approaches in absolute quantitative proteomics with mass spectrometry," *Mass Spectrom. Rev.*, vol. 37, no. 6, pp. 715–737, 2018.

[7] Crustal Geophysics and Geochemistry Science Center, "No Title." [Online]. Available: https://crustal.usgs.gov/.

[8] Howard E.Taylor, *Inductively Coupled Plasma - Mass Spectrometry: Practices and Techniques*. 2000.

[9] S. M. Nelms, *Inductively Coupled Plasma Mass Spectrometry Handbook*. 2009.

[10] R. Gilstrap, "A colloidal nanoparticle form of indium tin oxide : system development and characterization SYSTEM DEVELOPMENT AND CHARACTERIZATION Presented to The Academic Faculty by Richard Allen Gilstrap Jr . In Partial Fulfillment of the Requirements for the Degree ," no. January 2009, 2018.

[11] https://www.labcompare.com/347319-Routine-Maintenance-in-ICP-MS-Critical-When-Monitoring-Elemental-Impurities-in-Pharmaceuticals/. [10.01.2019]

[12] https://community.asdlib.org//imageandvideoexchangeforum/files/2013/07/Figure10.58.jpg [10.01.2019].

[13] https://crustal.usgs.gov/laboratories/icpms/intro.html [10.01.2019].

[14] https://www.shimadzu.com/an/hplc/support/lib/lctalk/61/61intro.html. [12.03.2019]

[15] https://appliedspectra.com/edible-salt-classification.html/laser-ablation-chamber [12.03.2019].

[16] D. J. Hare, J. Lear, D. Bishop, A. Beavis, and P. A. Doble, "Protocol for production of matrix-matched brain tissue standards for imaging by laser ablation-inductively coupled plasma-mass spectrometry," *Anal. Methods*, vol. 5, no. 8, pp. 1915–1921, 2013.

[17] M. Šala, V. S. Šelih, and J. T. Van Elteren, "Gelatin gels as multi-element calibration standards in LA-ICP-MS bioimaging: Fabrication of homogeneous standards and microhomogeneity testing," *Analyst*, vol. 142, no. 18, pp. 3356–3359, 2017.

[18] M. Bonta, H. Lohninger, M. Marchetti-Deschmann, and A. Limbeck, "Application of gold thin-films for internal standardization in LA-ICP-MS imaging experiments," *Analyst*, vol. 139, no. 6, pp. 1521–1531, 2014.

[19] https://www.fluidigm.com/binaries/content/documents/fluidigm/resources/maxpar-antibody-labeling-kit-pr-prd002/maxpar-antibody-labeling-kit-pr-prd002/fluidigm%3Afile. [28.02.2019]

[20] https://en.wikipedia.org/wiki/Neodymium.[28.02.2019]

[21] https://www.inorganicventures.com/icp-ms-measurement [28.02.2019].

[22] https://www.lenntech.de/data-pse/ionisierungsenergie.htm. [28.02.2019]

[23] https://www.internetchemie.info/chemische-elemente/seltene erden.php [28.02.2019].

[24] D. A. Frick and D. Günther, "Fundamental studies on the ablation behaviour of carbon in LA-ICP-MS with respect to the suitability as internal standard," *J. Anal. At. Spectrom.*, vol. 27, no. 8, pp. 1294–1303, 2012.

[25] H. J. Finley-Jones, J. L. Molloy, and J. A. Holcombe, "Choosing internal standards based on a multivariate analysis approach with ICP(TOF)MS," *J. Anal. At. Spectrom.*, vol. 23, no. 9, pp. 1214–1222, 2008.

[26] https://www.proteinatlas.org/learn/method/immunohistochemistry [15.02.2019].

[27] T. W. Jacobs, E. John, I. E. Stillman, and S. J. Schnitt, "Loss of tumor marker-immunostaining intensity of stored paraffin slides of breast cancer," vol. 88, no. 15, 1996.

[28] U. Manne, R. B. Myers, S. Srivastava, and W. E. Grizzle, "Re: loss of tumor marker-immunostaining intensity on stored paraffin slides of breast cancer.," *J. Natl. Cancer Inst.*, vol. 89, no. 8, pp. 585–586, 1997.

[29] https://www.selectscience.net/products/icap-q-icp-ms/?prodID=194942 [13.02.2019]..

[30] http://www.nwrlasers.com/laserablation/nwr213/. [15.02.2019].

[31] https://www.thermofisher.com/order/catalog/product/957250 [15.02.2019]..

[32] Available: http://www.statistics4u.info/ [15.02.2019]..

[33] https://www.abcam.com/protocols/immunostaining-paraffin-frozen-free-floating-protocol#Free-floating sections. [17.02.2019].

[34] D. P. Bishop, N. Cole, T. Zhang, P. A. Doble, and D. J. Hare, "A guide to integrating immunohistochemistry and chemical imaging," *Chem. Soc. Rev.*, vol. 47, no. 11, pp. 3770–3787, 2018.

[35] https://www.thermofisher.com/order/catalog/product/D1306 [17.02.2019]..

[36] Fluidigm, "MAXPAR ® Antibody Labeling Kit Protocol," vol. PRD002, no. Version 7 Protocol, pp. 1–6, 2017.

[37] E. Pérez, K. Bierla, G. Grindlay, J. Szpunar, J. Mora, and R. Lobinski, "Lanthanide polymer labels for multiplexed determination of biomarkers in human serum samples by means of size exclusion chromatography-inductively coupled plasma mass spectrometry," *Anal. Chim. Acta*, vol. 1018, pp. 7–15, 2018.

[38] M. Cruz-Alonso, A. Lores-Padín, E. Valencia, H. González-Iglesias, B. Fernández, and R. Pereiro, "Quantitative mapping of specific proteins in biological tissues by laser ablation–ICP-MS using exogenous labels: aspects to be considered," *Anal. Bioanal. Chem.*, vol. 411, no. 3, pp. 549–558, 2019.

[39] M. Bonta, "Elemental imaging using LA-ICP-MS on biological samples," *Tech. Univ. Wien*, 2013.

[40] L. Waentig, N. Jakubowski, S. Hardt, C. Scheler, P. H. Roos, and M. W. Linscheid, "Comparison of different chelates for lanthanide labeling of antibodies and application in a Western blot immunoassay combined with detection by laser ablation (LA-)ICP-MS," *J. Anal. At. Spectrom.*, vol. 27, no. 8, pp. 1311–1320, 2012.